Biosensors and Bioelectronics 132 (2019) 143–161

Contents lists available at ScienceDirect

Biosensors and Bioelectronics

journal homepage: www.elsevier.com/locate/bios

Specific and label-free immunosensing of protein-protein interactions with silicon-based immunoFETs

Ie Mei Bhattacharyya[a,1], Shira Cohen[b,1], Awad Shalabny[c], Muhammad Bashouti[c,d], Barak Akabayov[b], Gil Shalev[a,d,*]

[a] Department of Electrical & Computer Engineering, Ben-Gurion University of the Negev, POB 653, Beer-Sheva 8410501, Israel
[b] Department of Chemistry, Ben-Gurion University of the Negev, POB 653, Beer-Sheva 8410501, Israel
[c] Jacob Blaustein Institutes for Desert Research, Seder Boqer Campus, Ben-Gurion University of the Negev, 8499000 Sede Boqer, Israel
[d] The Ilse-Katz Institute for Nanoscale Science & Technology, Ben-Gurion University of the Negev, POB 653, Beer-Sheva 8410501, Israel

ARTICLE INFO

Keywords:
ImmunoFET
Label-free
Specific
Immunosensing
Protein-protein interactions
ISFET
pH sensitivity

ABSTRACT

The importance of specific and label-free detection of proteins via antigen-antibody interactions for the development of point-of-care testing devices has greatly influenced the search for a more accessible, sensitive, low cost and robust sensors. The vision of silicon field-effect transistor (FET)-based sensors has been an attractive venue for addressing the challenge as it potentially offers a natural path to incorporate sensors with the existing mature Complementary Metal Oxide Semiconductor (CMOS) industry; this provides a stable and reliable technology, low cost for potential disposable devices, the potential for extreme minituarization, low electronic noise levels, etc. In the current review we focus on silicon-based immunological FET (ImmunoFET) for specific and label-free sensing of proteins through antigen-antibody interactions that can potentially be incorporated into the CMOS industry; hence, immunoFETs based on nano devices (nanowire, nanobelts, carbon nanotube, etc.) are not treated here. The first part of the review provides an overview of immunoFET principles of operation and challenges involved with the realization of such devices (i.e. e.g. Debye length, surface functionalization, noise, etc.). In the second part we provide an overview of the state-of-the-art silicon-based immunoFET structures and novelty, principles of operation and sensing performance reported to date.

1. Introduction

Immunosensors are bio-affinity ligand-based devices, which rely on the naturally occurring activation of the adaptive immune system. In this process, biomolecular targets (antigens) initiate the immune response to produce antibodies that identify and neutralize the antigens via the formation of specific and stable antigen-antibody complexes. In nature, antigens are usually proteins and peptides and the interaction between antibodies and proteins is classified as protein-protein interaction (PPI). Nonetheless, polysaccharides, DNA and other biomolecules may also serve as antigens. Antibodies are Y-shaped glycoproteins composed of four peptide chains - two heavy chains and two light chains - which specifically bind to the targeted antigens by identification of a 3-D structural pattern (epitope). Antibodies can be either

Abbreviations: ACTH, Adrenocorticotropin; AMFET, Accumulation mode Field effect transistor; APS, Aminopropylsilane; APTES, Aminopropyltriethoxysilane; APTMS, Aminopropyltrimethoxysilane; BSA, Bovine serum albumin; CG, Control gate; CMOS, Complementary Metal Oxide Semiconductor; CνMOS, Chemoresistive neuron metal oxide semiconductor; DGFET, Double gate Field effect transistor; DMFET, Dielectric modulated Field effect transistor; DNA, Deoxyribonucleic Acid; EDL, Electric Double Layer; EFN, Electrostatically formed Nanowires; EGFET, Extended gate Field effect transistor; EGOFET, Electrolyte-gated Organic Field Effect Transistor; EIA, Enzyme-immunoassays; EIS, Electrolyte-Insulator-Semiconductor; ELISA, Enzyme linked immunosorbent assay; FD, Fully depleted; FET, Field Effect Transistor; FG, Floating gate; FIA, Fluoroimmunoassays; GA, Glutaraldehyde; HEMT, High Electron Mobility Transistor; HSA, Human Serum Albumin; IRUS, Ion-responsive urine sensor; ISFET, Ion Sensitive Field Effect Transistor; ITO, Indium Tin Oxide; JL-DG-DMFET, Junction less dual gate dielectric modulated Field effect transistor; LOD, Limit of detection; MOSFET, Metal Oxide Semiconductor Field Effect Transistor; OFET, Organic Field Effect Transistor; PBS, Phosphate Buffer Solution; PDGF, Platelet-derived growth factor; PPI, Protein-protein Interaction; PSMA, Poly(styrene-*co*-methacrylic acid); PVB, Polyvinylbutyral; RCA, Rolling circle amplification; RIA, Radioimmunoassay; SAM, Surface assembled monolayer; SBP, Silicon binding proteins; SiNW, Silicon nanowires; SNR, Signal-to-noise ratio; SOI, Silicon-On-Insulator; TFET, Tunneling Field effect transistor

* Corresponding author at: Department of Electrical & Computer Engineering, Ben-Gurion University of the Negev, POB 653, Beer-Sheva 8410501, Israel.
E-mail address: glshalev@bgu.ac.il (G. Shalev).
[1] Equal contributor.

https://doi.org/10.1016/j.bios.2019.03.003
Received 25 December 2018; Received in revised form 3 March 2019; Accepted 4 March 2019
Available online 05 March 2019
0956-5663/

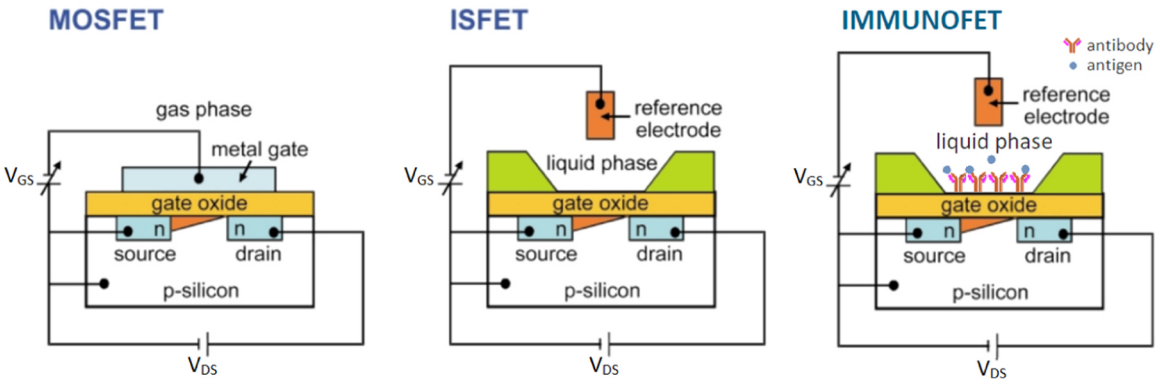

Fig. 1. Schematic illustrations of MOSFET, ISFET and immunoFET. V_{GS} denotes the gate voltage and V_{DS} denotes the source-drain voltage. The ISFET is realized by replacing the MOSFET metal gate with a reference electrode immersed in an electrolyte. The immunoFET is realized by immobilizing antigen-specific antibodies on the gate oxide of the ISFET for antigen detection. Adapted from Hierlemann and Baltes (2003).

monoclonal or polyclonal depending whether they target a specific epitope presented by an antigen, or target multiple patterns of the antigen, respectively. While antigen-antibody interactions are mediated through weak non-covalent bonds such as electrostatic bonds, hydrogen bonds and hydrophobic interactions, antibodies' affinity toward their antigens is one of the strongest known in nature and can get to dissociation constant (K_d) values of less than a nanomolar (Boder et al., 2000; Friguet et al., 1985).

Due to their very high affinity, specificity, structural stability and their non-covalent binding to their targets, antibodies are broadly utilized in scientific research for plethora of applications, including the separation and isolation of biomolecules, detection of biomolecules in samples, quantitative and qualitative analysis, and localization of antigens in complexed systems. Techniques based on antigen-antibody interactions have been a well-established practice for many decades in biological research, and the development of immunosensors is considered a significant milestone in the field of clinical bioanalytics. Immunosensors are used in a wide spectrum of applications ranging from healthcare, food processing and safety, environmental control to security and defense.

Immunosensors are classified into two types: labeled and label-free. Label-based immunosensors use "tags" or labels with specific properties to detect the targeted antigen in a mixture of other biomolecules by measuring the immunochemical reaction. Several types of labels have been investigated and used in biological research over the years. The first label to be used were radioisotopes in radioimmunoassays (RIA) which laid the foundation for further development of other types of tagged-immunoassays. Frequently used tags are: (1) enzymes in enzyme-immunoassays (EIA), (2) bacteriophages in viroimmunoassays, (3) fluorescent group in fluoroimmunoassays (FIA) and (4) stable free-radical in spin-immunoassays (Wisdom, 1976). A commonly used label-based immunosensor is the enzyme-linked immunosorbent assay (ELISA) that was developed in 1971 (Engvall and Perlmann, 1971). The ELISA is based on enzyme-labeling of the antibody instead of isotope-labeling as performed in RIA (Yalow and Berson, 1960). Biological detection using immunoassays requires to differentiate the bound fraction (antibody-antigen complex) from the unbound fraction (free antigen or antibody) depending on the type of immunoassay: heterogeneous or homogeneous. ELISA, being a heterogeneous type of enzyme immunoassay requires the antigen-antibody complexes formed after incubation to be physically separated from free unbound antibodies using several washing steps (Engvall, 1980). After the isolation of the antigen-antibody complex, a tagged secondary antibody is added to bind the primary antibody. The enzyme tag catalyzes colorimetric reactions and enables the quantification of antigen in the sample. ELISA is one of the most extensively used immunoassay especially for protein analytes. Ever since its inception, ELISA has evolved and detection limit as low as 5 pg/mL was recently reported for detection of tumor suppressor protein p53 (Jia et al., 2009). ELISA immunosensors are both reliable and highly sensitive. However, they suffer from drawbacks such as the demand for relatively large sample volumes, long incubation periods, sophisticated laboratory apparatus, highly skilled laboratory staff, and multiple labeling strategies that would not interfere with the antigen-antibody interactions. On the other hand, label-free detection allows the direct monitoring of the physicochemical or electrical changes induced by the antigen-antibody complex formation. Different label-free detection techniques have been reported which include mass spectrometry, micro-cantilevers, quartz crystal microbalance, surface plasmon resonance, anomalous reflection of gold, etc (Broeck et al., 2015; Mousavi et al., 2015; Pirincci et al., 2018; Sipova et al., 2010; Watanabe et al., 2005; Zhou et al., 2016). Label-free assays can show biologically active molecular interactions and cellular responses, give comprehensive information on the specificity, affinity and in many cases, also the binding kinetics and thermodynamics (Chan et al., 2016; Jin et al., 2017; Li et al., 2015) (Note that the concepts of selectivity and specificity are used interchangeably in the case of immunosensing. However, specificity is regarded as an intensification of selectivity, viz. the ultimate of selectivity. In the current review we mostly adapt the convention used by the cited works).

Bergveld introduced the ion-sensitive field effect transistors (ISFET) in 1970 around the same time ELISA was developed and has been since successfully utilized for pH sensing; the ISFET is based on the coupling of ionic activities in electrochemical or biological environment with the field-effect modulation principle (Bergveld, 1970). The ISFET architecture is similar to that of a conventional MOSFET with the metal gate electrode replaced with a reference electrode immersed in a solution, which is in contact with the gate insulator. The ISFET is the progenitor to the more evolved immunoFET device, which in its most basic form is an ISFET with the active surface modified with antibodies. The specific interaction of the surface-bound antibodies and the target proteins is expected to induce an electrostatic perturbation that affects the immunoFET threshold voltage and, consequently, the drain-source current (I_{DS}). Fig. 1 presents a structural comparison to visualize the realization of an immunoFET from a conventional MOSFET and ISFET. Schenk was the first to utilize the ISFET platform for the measurement of proteins via their intrinsic charges where he demonstrated two cases (Schenck, 1978). Initially, the specific sensing of human serum albumin (HSA) was demonstrated using surface-immobilized antibodies in NaCl solution by monitoring I_{DS}. Next, insulin, thyroglobulin and adrenocorticotropin (ACTH) were used as antigens on the same device to form "immunological integrated circuit", and measurements of multiple antigens were performed. Gotoh et al. demonstrated one of the earliest immunoFETs in which anti-human serum albumin (anti-HSA) immunoglobulin G (IgG) was immobilized on a polyvinylbutyral (PVB)

membrane placed on an ISFET-sensing channel for label-free detection of HSA (Gotoh et al., 1989). Sensor signal was linear with HSA concentration over a range of 0.01–1.0 mg mL^{-1}. Silicon has been the primary choice of semiconducting material for transistor-based biosensors as the technology has significantly matured over the decades and hence can support immunoFET technologies with low noise levels, stable and robust fabrication processes suitable for low-cost (potential for disposable sensors) and mass production.

Still, although the straightforward rational and seeming simplicity of the immunoFET, not many successes have been reported in the literature for specific and label-free sensing of proteins. The goal of the present review is to report the state-of-the-art of silicon-based immunoFET for specific and label-free sensing of protein antigens via interactions with the immobilized antibody. The review starts with the immunoFET principle of operation and we summarize the main obstacles and challenges associated with the Debye screening length, passivation, leakage current and noise. The main part of the review provides an overview of the main silicon-based immunoFET designs reported to date.

2. ImmunoFET: detection principles, concerns and challenges

The immunoFET is derived from the ISFET by functionalizing the oxide surface with antibodies to make it sensitive to antigens. In the following section, we briefly discuss the operation principle of the ISFET followed by the immunosensing mechanism of the immunoFET. We also discuss the main challenges and obstacles concerning the Debye screening length, surface functionalization, passivation, gate dielectric materials and noise, which are fundamental concerns affecting and determining the specific and label-free detection capabilities and performance of FET-based immunosensors.

2.1. ISFET: principle of operation

Fig. 2 presents a typical ISFET, which is the combination of an electrolyte-insulator-semiconductor (EIS) interface with an underlying FET. The pH sensitivity of the ISFET is shaped by the interaction of the oxide surface with the electrolyte. Upon introduction of a solution to the oxide surface, the SiOH surface hydroxyl groups can either donate or accept protons depending on the local surface pH level and, respectively, leave a negatively or positively charged surface group. The site binding model describes the equilibrium reactions between the so-called amphoteric SiOH surface sites and the H^+ ions in the solution responsible for the oxide surface charge. In the below we follow the ISFET pH sensitivity derivation as proposed by Bergveld (2003). The

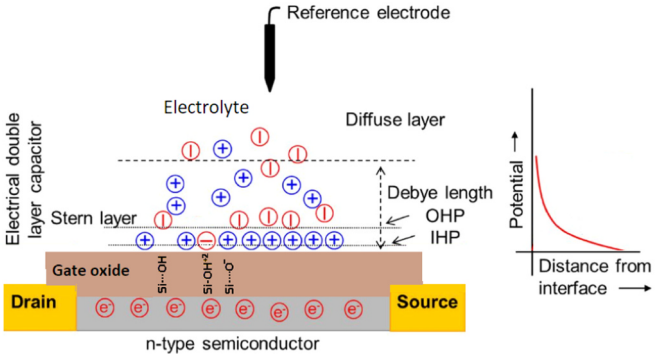

Fig. 2. An illustration of an ISFET with the formation of an EDL at the oxide-electrolyte interface. The (de)protonation of SiOH surface hydroxyl groups creates amphoteric sites (SiO^- or $SiOH^{+2}$) on the oxide surface. EDL consists of the Stern layer and the diffuse layer. The Stern layer is made of the inner Helmholtz layer (IHP) and the outer Helmholtz layer (OHP). The potential drops exponentially towards zero with distance. Adapted from Pachauri and Ingebrandt (2016).

reactions are:

$$SiOH \Longleftrightarrow SiO^- + H_B^+, \tag{1}$$

$$SiOH_2^+ \Longleftrightarrow SiOH + H_B^+, \tag{2}$$

where $H_B{}^+$ denote the protons in the bulk solution. These equilibrium reactions build up a net surface charge density σ_0. In order to sustain the requirement for charge neutrality at the oxide-electrolyte interface, the surface charge density σ_0 is balanced by an equal and opposite charge σ_{dl} in the electrolyte ($\sigma_{dl} = -\sigma_0$), leading to the formation of electric double layer.

The electric double layer formed at the oxide-electrolyte interface is described by the Gouy-Chapman-Stern model as illustrated in Fig. 2. The Stern layer (also known as the Helmholtz layer) is the layer closest to the oxide surface which contains solvent molecules that are adsorbed on the oxide. The charged oxide surface, due to surface (de)protonation, attracts the solution counter-ions towards the interface and, on the other hand, depletes the surface of co-ions, and in this manner creates the diffuse layer or the Gouy–Chapman layer (Bard and Faulkner, 2001). The ability of the double layer to store charge in response to a small change in the potential $\partial\sigma_0/\partial\Psi_0$ is defined as the differential double-layer capacitance, C_{diff}, and is given by:

$$\frac{\partial\sigma_0}{\partial\Psi_0} = -\frac{\partial\sigma_{dl}}{\partial\Psi_0} = C_{diff}. \tag{3}$$

The ISFET behavior is primarily attributed to the surface potential Ψ_0 developed at the oxide-electrolyte interface. The threshold voltage (V_T) of the ISFET relates to Ψ_0 in the following manner:

$$V_T = V_{REF} - \Psi_0 + \chi_{sol} - \frac{\Phi_{Si}}{q} - \frac{Q_{ss} + Q_{ox}}{C_{ox}} - \frac{Q_B}{C_{ox}} + 2\phi_F, \tag{4}$$

where Q_B is the depletion charge in silicon, ϕ_F is the Fermi potential, V_{REF} is the reference electrode potential relative to vacuum, Φ_{Si} is the silicon work function, C_{ox} is the gate dielectric capacitance, Q_{ss} is the surface state density and Q_{ox} is the fixed oxide charge. The interface potential at the gate dielectric-electrolyte interface is determined by Ψ_0 and the surface dipole potential of the solution χ_{sol}. Thus, any variation in Ψ_0 causes a corresponding change in the V_T, making ISFET sensitive to the pH levels of the electrolyte.

The redistribution of ions close to the electrolyte-oxide interface is described by Boltzmann equation:

$$pH_s = pH_b + \frac{e\Psi_0}{2.3kT}, \tag{5}$$

where pH_s and pH_b are the pH at the surface and at the bulk, respectively. Thus, a change in the bulk pH (ΔpH_b) is compensated by a change in the surface pH (ΔpH_s) and the surface potential Ψ_0. The surface hydroxyl groups should effectively buffer the oxide surface as determined by the intrinsic buffer capacity $\beta_{int} = \frac{\partial B}{\partial pH_s}$, where B is the difference between the number of negatively charged groups and the positively charged groups in moles per unit area. This maintains almost constant ΔpH_s such that ΔpH_b is fully compensated by Ψ_0, which is the Nernst response and is given by

$$\frac{\partial\Psi_0}{\partial pH_b} = -\frac{2.3kT}{q}\alpha, \tag{6}$$

$$\alpha = \frac{1}{1+\frac{2.3kTC_{diff}}{q^2\beta_{int}}}, \tag{7}$$

where α is a dimensionless sensitivity parameter ranging between 0 and 1, depending on β_{int} and C_{diff}. The maximum pH sensitivity is achieved for α = 1 which is the so-called Nernst sensitivity of −59.2 mV/pH.

Recently, Parizi et al. reported that the ISFET pH sensitivity can be significantly enhanced beyond the Nernst limit by using pH buffer solutions containing counter ions that exceed a specific size (Parizi et al., 2017). They proposed a modified Boltzmann model that considers the

non-trivial ion size:

$$\frac{d\Psi_0}{dpH_b} = -2.3\frac{kT}{q}\left(\frac{1}{1+\alpha-\delta}\right), \tag{8}$$

$$\delta = \frac{2a^3c_B\sinh\left(\frac{q\Psi_0}{kT}\right)}{1+4a^3c_B\sinh^2\left(\frac{q\Psi_0}{2kT}\right)}, \tag{9}$$

where a is the ion size, c_B is the bulk concentration of the counter-ions and δ is a dimensionless sensitivity parameter ranging between 0 and 1. Thus, a large enough counter-ion size will give higher δ value, resulting in pH sensitivity exceeding the Nernst limit. They presented experimental results using an extended gate ISFET and showed that the sensitivity increased to around ~220 mV/pH for pH 10 and estimated ionic size of ~10 Å.

2.2. Immunosensing with ImmunoFET

The charge of a molecule is determined by its atomic composition and its solvent properties. As mentioned earlier, antibodies can detect and bind to spatial patterns of biomolecules such as DNA and proteins. The change in charge of the antigen-antibody complex relies on chemical properties of the antigen and antibody in physiological conditions (Reverberi and Reverberi, 2007). Proteins are biopolymers composed of amino acids. The amino acid sequence determines the structure and conformation of a protein in considerations with the environmental conditions (such as pH levels, temperature, presence of other compounds, etc.). The amino acid sequence also determines the isoelectric point (*pI*) of the protein which is the theoretical pH value in which the molecule carries zero electrical charge.

When an antibody (*Ab*) having a charge X_1 undergoes an immunological reaction with an antigen (*Ag*) having charge X_2, an antibody-antigen complex is formed having total charge X_3:

$$Ab^{X_1} + Ag^{X_2} \overset{K}{\Leftrightarrow} [AbAg]^{X_3}. \tag{10}$$

It is expected that the charge difference from X_1 to X_3 can be measured by the immunoFET. The change in the charge density at the gate oxide/solution interface induces an equal charge density change of opposite sign in the semiconductor/oxide interface, which affects the threshold voltage of the immunoFET.

Various attempts were reported to provide a theoretical infrastructure of immunoFET. Wunderlich et al. analytically demonstrated that the pH sensitivity of immunoFETs can decrease or even suppress the measured signal for protein adsorption (Wunderlich et al., 2007). They reported that the electrolyte concentration n_o and the charge sensitivity are related to the pH sensitivity via the sensitivity parameter α. The sensitivities of Ψ_0 to n_o and to analyte charge $\sigma_{analyte}$ are given by:

$$\frac{d\Psi_0}{dn_0} = \left(\frac{\partial\Psi_0}{\partial n_0}\right)_{\sigma_0}(1-\alpha), \tag{11}$$

$$\frac{d\Psi_0}{d\sigma_{analyte}} = \left(\frac{d\Psi_0}{d\sigma_0}\right)_{n_0}\left(\frac{d\sigma_0}{d\sigma_{analyte}}\right)_{\sigma_{protons}}(1-\alpha), \tag{12}$$

where the total surface charge density σ_0 is the sum of $\sigma_{analyte}$ and the acid-base charge $\sigma_{protons}$. Evidently, the above suggests that a high pH sensitivity reduces other sensitivities. For instance, a positive signal caused by the adsorption of positive charge induces a rise in the surface potential. This rise in the surface potential is accompanied by a decrease in pH_s, which causes more surface groups to dissociate—the surface becomes more negative and the surface potential is consequently decreased, and therefore the original positive charge adsorption signal is reduced. But, on the other hand, Shalev et al. experimentally examined the correlation between pH sensing and immunosensing using a double-gate immunoFET, and demonstrated direct correlation between pH sensitivity and immunosensing (Shalev et al., 2012). They reported that the highest and lowest threshold voltage shift for a label-free and specific detection of 6.5 nM IgG were 40 mV and 2.3 mV with pH sensitivity of 35 mV/decade and 15 mV/decade, respectively.

Moreover, after surface functionalization of the immunoFET with antibodies, the residual hydroxyl groups on the active area may also limit the sensor response to the targeted antigens. Stoop et al. identified the residual pH response as a key factor limiting the sensor response and investigated the influence of a competing surface reaction on the specific detection of the targeted species (Stoop et al., 2015). They reported that the measurement of the targeted analyte $A_1{}^+$ suffers from the competing reaction with species $A_2{}^+$ and results in a nonlinear coupling between the targeted and the competing reactions via Ψ_0. The strength of this coupling is given by the ratio of the number of surface sites $\frac{N_2}{N_1}$. If one species dominates ($N_2 >> N_1$), the sensor will respond strongly to competing species A_2 while its response to targeted species A_1 is fully suppressed. They demonstrated the influence of pH on the sensor response to calcium ions using Ca^{2+}-sensitive receptor molecules on gold-coated nanoribbons. Including the Boltzmann distribution for both protons and Ca^{2+}, they derived Ψ_0 as

$$\Psi_0 = 2e\frac{N_{Ligand}}{C_{dl}}\left(\frac{a_{Ca^{2+}}}{a_{Ca^{2+}} + K_{Ligand}e^{2e\Psi_0/kT}} - 1\right) + e\frac{N_s}{C_{dl}}\frac{a_{H^+}^2 - K_aK_be^{-2e\Psi_0/kT}}{a_{H^+}^2 - a_{H^+}K_be^{e\Psi_0/kT} + K_aK_be^{2e\Psi_0/kT}}, \tag{13}$$

where C_{dl} is the double layer capacitance per unit area, N_{Ligand} and N_s are the total number of surface sites per unit area for ligand and hydroxyl groups respectively, $a_{Ca}{}^{2+}$ and $a_H{}^+$ are activity of calcium ions and protons respectively and K_{Ligand}, K_a and K_b are the dissociation constants. The first term of Eq. (13) is due to the functionalized groups and the second term relates to the intrinsic pH sensitivity. They presented experimental results to show that the pH value determined the total shift in potential $\Delta\Psi_{total}$ due to $a_{Ca}{}^{2+}$ and the region of maximum response.

Landheer et al. proposed immunoFET theoretical model based on the Donnan potential (Landheer et al., 2005). They considered the layer of biological macromolecules as an ion-permeable membrane and modified the expression for Ψ_0 of an ISFET to include terms involving the semiconductor surface charge and the Donnan potential Ψ_{DP} (potential in the bulk of an ion-permeable membrane where charge neutrality prevails) of the ion-permeable membrane:

$$\Psi_0 = \frac{4.606qN_s\left(\frac{K_b}{K_a}\right)^{\frac{1}{2}}(pH_{pzc} - pH) + C_{LDL}\Psi_{DP} + \sigma_s}{2q^2N_s\left(\frac{K_b}{K_a}\right)^{\frac{1}{2}}/kT + C_{LDL}}, \tag{14}$$

$$\frac{1}{C_{LDL}} = \frac{1}{C_{Stern}} + \frac{kT}{zq(2\varepsilon_m kTn_0)^{1/2}}, \tag{15}$$

where ε_m is the permittivity of the membrane, pH_{pzc} is the isoelectric point of the targeted antigen, C_{LDL} is the linearized double layer capacitance, C_{Stern} is the Stern layer capacitance, N_s is the number of surface sites per unit area, and z is the equal valence (a z: z electrolyte). In the limit of an uncharged surface, $\Psi_0 = \Psi_{DP} + \sigma_s/C_{LDL}$, and therefore Ψ_0 tracks Ψ_{DP}. They showed that the increase in the membrane charge density dramatically reduces the change in Ψ_0 compared to an uncharged surface due to presence of amphoteric sites on the oxide surface. Also, for higher ionic concentrations, the variation of Ψ_0 decreases for both uncharged and charged oxide surface reflecting low Donnan potentials, low surface potentials and low membrane charge.

2.3. Debye screening length

The electrostatic potential of an analyte in an electrolyte is screened by the presence of other charges in the electrolyte. The Debye length

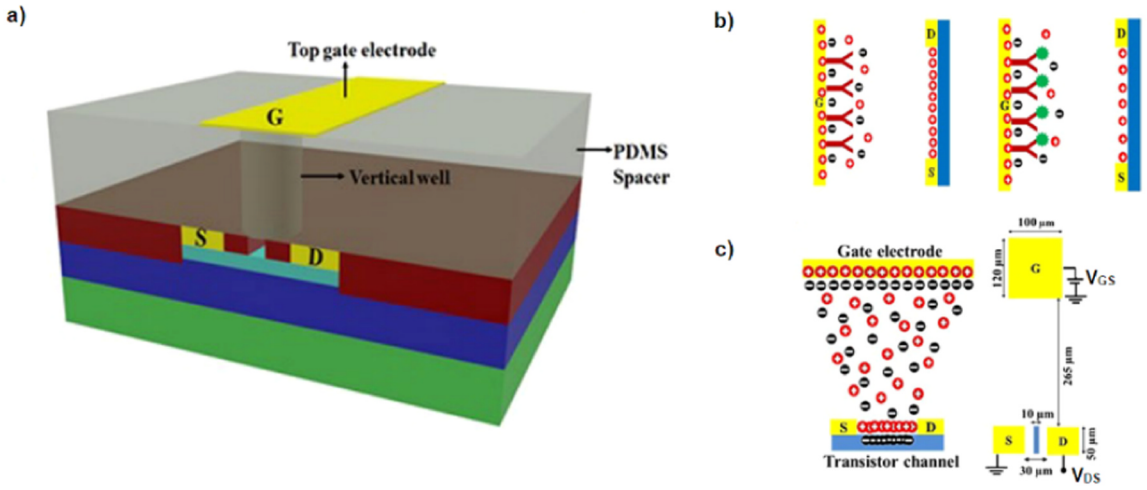

Fig. 3. a) A schematic model of the HEMT-based EDL-FET. **b)** A schematic representation of the top gate electrode immobilized with antibodies. Binding of antigens to the electrode-bound antibodies entails gate voltage drop and redistribution of the local charge density at the gate electrode leading to subsequent changes in the charge density on the active area of the FET. **c)** Distribution of ions under positive gate bias. Typical area of gate electrode opening is 100 μm × 120 μm, distanced at 265 μm from the active channel. Copied from Chu et al. (2017). Copyright © 2017, Springer Nature.

(λ_D) quantifies this screening length and is defined as:

$$\lambda_D = \sqrt{\frac{\varepsilon kT}{e^2 \sum_i N_A c_i z_i^2}}, \tag{16}$$

where e is the proton charge, ε is the permittivity of the solvent, N_A is the Avogadro's number, z_i and c_i are the valence and concentration of ion species i, respectively, and the sum extends over all ion species in solution (J. Israelachvili, 1991). Therefore, theoretically, any binding event that occurs at a distance from the electrolyte/oxide interface that is greater than λ_D will not be detected by the immunoFET. In order to circumvent the obstacle of the Debye length, the sensing measurements are carried out in diluted buffer solutions. This, however, can potentially affect protein conformation and result in subsequent loss of protein activity and binding affinity, as the structure of proteins is highly dependent on environmental conditions supplied by their solvent (as in secondary structures that are based on hydrogen bonds and tertiary and quaternary structures that rely on electrostatic and hydrophobic interactions) (Chu et al., 2017).

Stern et al. demonstrated specific and label-free protein detection using nanowire-FET sensors and reported that the difference between the pH of the solution (pH_{sol}) and pI of the analyte, $|pH_{sol} - pI|$ should be maximized to optimize sensitivity (Stern et al., 2007a). Moreover, they proposed that the salt concentration of the buffer used for biological detection should be selected such that λ_D is sufficiently long to allow sensing and short enough to screen unbound macromolecules (Stern et al., 2007b). Recently, Shoorideh et al. numerically studied Debye screening in nanowire-FET biosensors. They demonstrated that due to the direction of the curvature in concave and convex surfaces, a patch of the surface of the concave electrode has a larger Debye volume (volume of electrolyte within one Debye length of a surface) than an equally sized patch on the convex electrode, even though the Debye lengths are the same. Thus, they concluded that Debye screening is stronger near convex surfaces compared to that near concave or flat surfaces due to a small surface area to Debye volume ratio (Shoorideh and Chui, 2014). In the case of nanowire sensors, this contradicts the prediction that downscaling of dimensions will improve sensitivity as shrinking the nanowire diameter will increase convexity resulting in increased Debye screening and reduced sensitivity.

To overcome the challenge of Debye screening, Palazzo et al. proposed immunosensing governed by the capacitive effect that is independent of the Debye length (Palazzo et al., 2015). The transfer characteristics are measured in the saturation regime where $I_{DS}{}^{sat}$ is given by (Horowitz, 1998):

$$I_{DS}^{sat} = \frac{\mu WC}{2L}(V_{GS} - V_T)^2, \tag{17}$$

where W and L are the channel width and length respectively, μ is the mobility and C is the total gate capacitance. Decoupling the capacitance and threshold voltage contributions, the immunoFET response can be written as

$$\frac{\Delta I}{I_0} = \frac{\Delta C}{C_0} + \frac{2\Delta V_T}{V_G - V_{T,0}}. \tag{18}$$

C is modeled as a series network of the fixed gate oxide capacitance (C_{fix}), the Donnan capacitance ($C_{DON} \propto$ ionic strength of the solution i_s) and the double layer capacitance ($C_{GCDL} \propto \sqrt{i_s}$) and a capacitance C_{par} in parallel to fully account for the stacked proteins and is written as:

$$C = \left(\frac{1}{C_{fix}} + \frac{1}{C_{GCDL}} + \frac{1}{C_{DON}}\right)^{-1} + C_{par}. \tag{19}$$

$\Delta C/C_0$ can be written as:

$$\frac{\Delta C}{C_0} = \left(\frac{C_0}{C_{fix}} + \frac{C_0\sqrt{\frac{kT}{\varepsilon\varepsilon_0}}}{\sqrt{i_s}} + \frac{C_0 g^{-1}}{i_s}\right) + \frac{C_{par}}{C_0} - 1, \tag{20}$$

where g is the proportionality constant linking C_{DON} to i_s. The capacitive immunoFET sensing mechanism is ascribed to the formation of Donnan equilibria within the protein layer, in series to the gate capacitance.

Another method for immunosensing beyond the Debye length was proposed by Chu et al. using ion-gated electric double layer FET (EDL-FET) (Chu et al., 2017). They demonstrated direct detection of HIV-1 RT, CEA, NT-proBNP and CRP in 1 × PBS (with 1% BSA) or human serum using antibody or aptamer immobilized AlGaN/GaN high electron mobility transistors (HEMT) as shown in Fig. 3a. The antibodies are immobilized on the gate electrode unlike in the conventional immunoFET as illustrated in Fig. 3b and the gate electrode is separated from the active channel of the FET as shown in Fig. 3a. The transfer characteristics are measured in the linear regime with I_{DS} given as:

$$I_{DS} = \frac{\mu WC_{ox}}{L}\left(V_{GS} - V_T - \frac{1}{2}V_{DS}\right)V_{DS} \tag{21}$$

where C_{ox} is the gate dielectric capacitance. The change in I_{DS} due to the protein binding is governed by the gate electrode opening and the gate voltage drop across the solution and the oxide. As shown in Fig. 3c,

larger gate electrode opening allows more ions to be attracted towards the gate opening. Consequently, this leads to more ions accumulating on the active area, thereby increasing the carrier concentration in the channel and the current gain as well. Moreover, when V_{GS} is applied to the gate electrode, the gate voltage drops through the solution (ΔV_s) and across the dielectric of the HEMT (ΔV_{ox}). The change in the solution capacitance C_s due to the target protein binding causes a change in the effective gate voltage as:

$$V_{GS} = \Delta V_s + \Delta V_{ox}, \tag{22}$$

$$\Delta V_{ox} = \frac{C_s}{C_s + C_{ox}} \times V_{GS}. \tag{23}$$

The gate voltage drop induced by the antibody-antigen reaction causes local charge redistribution at the gate electrode leading to subsequent changes in the charge density on the active channel as illustrated in Fig. 3b.

2.4. Surface functionalization

FET based immunosensing via adsorption of target biomolecules is translated to change in I_{DS} of the FET by the modification of the FET gate dielectric surface with a biomolecular layer as receptor. The immobilization of various biorecognition materials on the FET gate surface for biomarker analysis has been developed through surface modification technology. However, their viability for applications in immunosensing is defined by their 'specificity' which quantifies the ability of the sensor to detect extraordinarily low concentrations of a single target species in a complex biological environment. Conventionally, the specificity is introduced into the system with adequate chemical surface modification of the immunoFET active sensing area. Fig. 4(a) shows an immunosensor with antibodies immobilized on the surface. As demonstrated by Nair et al., when a solution containing antibodies is introduced onto the active area for surface functionalization, random attachment of the antibodies causes fragmentation of the active area for subsequent adsorption and forms voids as shown in Fig. 4(b). These voids allow non-specific binding [denoted as (B) in Fig. 4(c)] and physisorption of the parasitic molecules on the unpassivated regions [represented as (C) in Fig. 4(c)] which dramatically reduce the selectivity of the sensor. They presented a selectivity theory for label-free biosensors in which they used fundamental considerations of surface exclusion and diffusion limited transport to optimize the incubation time for effective surface functionalization. They also proposed a void distribution function to identify the dominant component of parasitic adsorption (Nair and Alam, 2010). They reported that a minimum bulk receptor concentration of 1 μM is required for a typical incubation time of 1 h to guarantee maximum surface coverage.

The layer with biorecognition materials is bridged to the FET gate dielectric via linker molecules which can be considered as a dipole on the surface. A promising approach is the utilization of polar monolayers to increase the electrostatic selectivity as it introduces a net electrical dipole perpendicular to the surface/interface. These polar monolayers modify the work function and electron affinity at a surface, and change the band offset and band bending at the interface (Bashouti et al., 2009; Khamaisi et al., 2010). This functionalization effect is a general one and can be obtained with non-molecular treatments as well. Nevertheless, the use of molecules, especially organic ones, allows a systematic tuning of the desired dipole moment by an appropriate choice of their functional groups or the intermolecular interactions between self-assembled molecules. As several functional groups can be attached to the same basic unit, optimal dipole design can be achieved together with optimal design of other pertinent chemical and (opto)-electrical properties, e.g., binding group(s), frontier orbital energy levels, etc. Due to the long range of the electrostatic phenomena, properties of polar monolayers are determined not only by the type of molecules and/or bonding configuration to the substrate, but also by size, (dis-)order, and adsorption patterns within the monolayer (Natan et al., 2007).

The dipole associated with a polar monolayer is usually modeled within the semi-classical Helmholtz picture, which effectively treats the monolayer as a dielectric "parallel plate-capacitor". However, significant difficulties in data interpretation within this simple picture have also been encountered (Kronik and Shapira, 1999). One example is the demonstrated modulation of current in the channel of a FET upon adsorption of a polar monolayer, where the molecular dipole substitutes or augments the transistor's gate. As there is no electric field outside a dipole layer in the parallel plate capacitor model, it is difficult to understand why this device works experimentally. Another example is the change observed in the current-voltage behavior of Schottky diodes possessing a polar monolayer at the metal/semiconductor interface which are inconsistent with the Helmholtz dipole at the interface (Haick et al., 2006; Natan et al., 2007).

The potential and field at a point $\vec{r}$ due to a point dipole $\vec{p}$ at the origin is respectively given by (For simplicity, we assume that the dipole is pointing in the z direction):

$$V(\vec{r}) = \frac{p\cos\theta}{r^2}, \quad E_r(\vec{r}) = \frac{2p\cos\theta}{r^3}, E_\theta(\vec{r}) = \frac{p\sin\theta}{r^3} \quad , \tag{24}$$

where V is the potential, E_r and E_θ are the electric field components in the direction of $\vec{r}$ and perpendicular to that direction, respectively, and θ is the polar angle (David and Jackson, 1999). When an array of dipoles is assembled, the potential and electric field simply add up

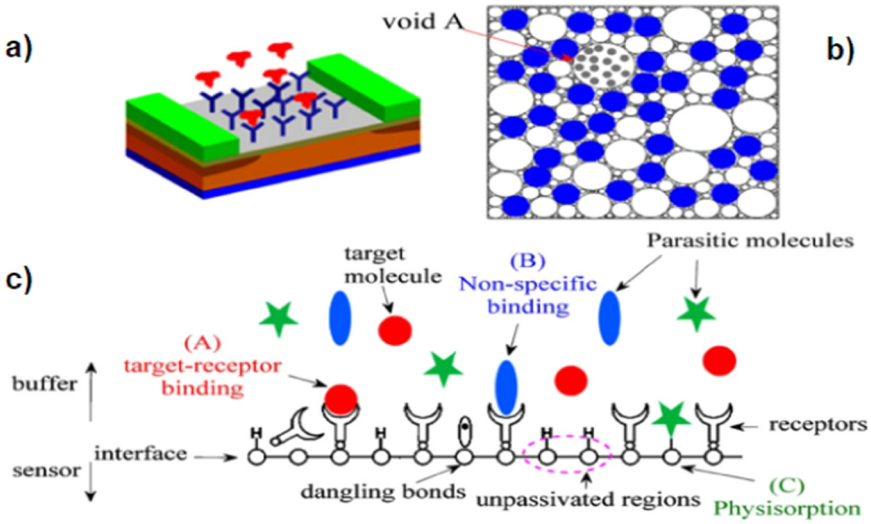

Fig. 4. a) A schematic of an immunosensor with surface-functionalized antibodies. **b)** Top view of the sensor active area shown in a). The blue solid dots represent the receptor molecules. The random attachment of receptors introduces voids (represented by white open circles) on the sensor surface over which parasitic adsorption can occur (illustrated as shaded small dots in the circle marked as void A). **c)** Cross-section of a sensor system illustrating the various components that contribute towards selectivity. Copied from Nair and Alam (2010). Rights managed by AIP publishing. (For interpretation of the references to color in this figure legend, the reader is referred to the web version of this article).

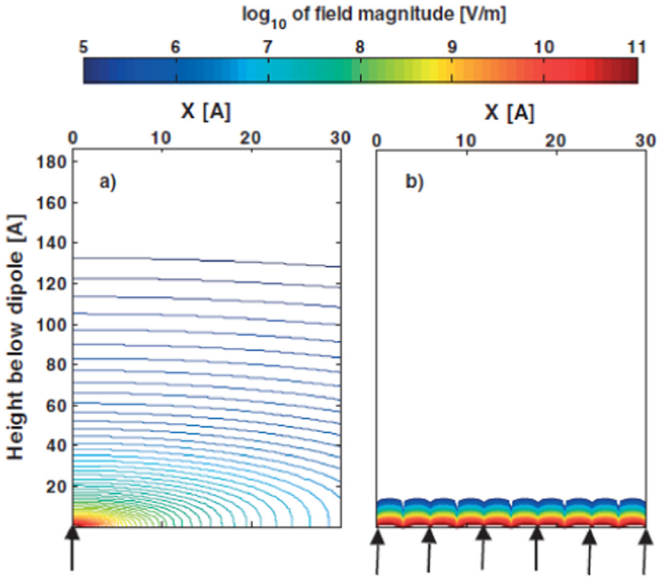

Fig. 5. Distribution of the electric field magnitude, on a logarithmic scale, in the xz plane due to: a) A single dipole with p = 4 Debye and d = 2 Å; b) A square array of such dipoles with inter-dipole separation of a = b = 6 Å. Dipole positions are indicated on the figure as arrows.

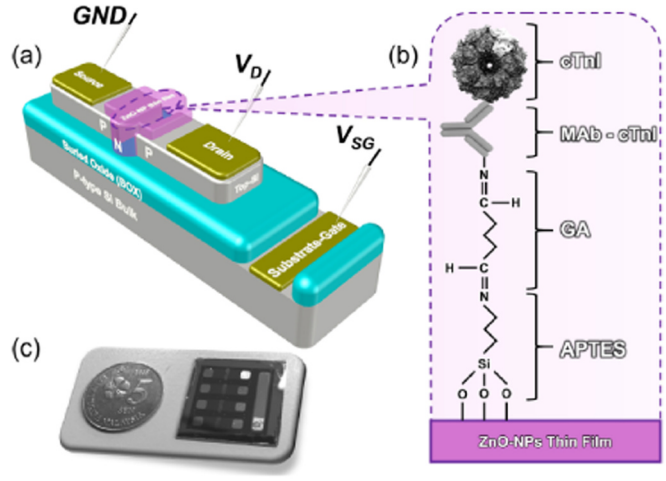

Fig. 6. Electrical detection of cTnI biomarker by ZnO-FET biosensor with substrate-gate coupling. (a) The 3D representation of the biosensor. (b) The surface functionalization of ZnO-NPs thin film with 3-aminopropyltriethoxysilane and glutaraldehyde; followed by surface immobilization process with cTnI monoclonal antibody for capturing cTnI biomarker. (c) The fabricated biosensor, comparable in size with Malaysia's 5 cent. Copied from Fathil et al. (2017). Copyright © 2016, Elsevier.

according to the superposition principle. However, since molecules are polarizable, their net dipole moment may change in response to external electric fields, such as those due to dipoles of other molecules. An illustration of this effect is given in Fig. 5, where the magnitude of the electrostatic field due to an isolated dipole and a planar dipolar array are compared. Surprisingly, the decrease in electric field is more pronounced for the dipolar layer than it is for the isolated dipole. Importantly, there exists a significant range of z values where the single dipole field is significant, but the monolayer field is negligible. This range of z values is inherently of the order of lateral dipole distances (compared the molecule length), as the vertical decay length, l_{max}, is proportional to the maximal lateral intermolecular distance.

After modifying the surface with a linker molecule, we may increase/decrease the sensitivity upon the adsorption of charged/non-charged target molecules. This is frequently encountered in the study of immunoFET based immunosensing. This is rationalized by the fact that the biomolecule (i.e. e.g. antibodies etc.) is considered a quadrupole (with or without net of charge) and therefore, the total potential is proportional to $1/r^5$. So, the sensing can be based on a combination of the following effects: (i) change in V_{th} (in case of flatband), which is due to the change in the vacuum level; (ii) the molecules (i.e. linker + antibody) behave as a molecular gate; and (iii) charge transfer between the surface and the molecules or even inside the molecules parallel to the channel (Chang et al., 2010). The first two effects can be tuned by internal interactions such as the density and the specific molecular orientation. For example to the first two effects, without specific orientation, H. Y. Lam demonstrated surface functionalization of a thin film with 3-aminopropyltriethoxysilane (APTES), followed by glutaraldehyde (GA) as a bi-functional linker to immobilize the cTnI monoclonal antibody (MAb-cTnI) as bio-receptor for capturing cTnI biomarker as illustrated in Fig. 6 (Fathil et al., 2017).

FET biosensors have been proved to be sensitive to the intrinsic electric charge of biomolecules. Cheng et al. showed that they can differentiate between two different tumors by immobilizing different antibodies on the FET gate and detected a specific tumor marker (Cheng et al., 2015). Few other studies also demonstrate immobilization of probes or receptors on aminosilane SAM-modified Si_3N_4/SiO_2 gate insulator; on a thiol SAM-modified gold electrode for extended gate; and on aminosilane SAM-modified SiO_2 gate insulator (Cheng et al., 2014; Goda and Miyahara, 2013; Hideshima et al., 2012; Hideshima et al., 2013a, 2013b; Niwa et al., 2005; Sakata et al., 2005; Sakata and Miyahara, 2005).

For the specific orientation, surface functionalization has been used to increase the sensitivity and LOD of immunoFETs. For example, attomolar detection of influenza A Virus Hemagglutinin Human H1 and Avian H5 was possible by using glycan-blotted FET biosensor (Hideshima et al., 2013a, 2013b). The small ligand glycans immobilized on the FET device, which make effective use of the charge-detectable region for FET-based detection in terms of Debye length, gave an advantage in the highly sensitive detection of the proteins – compared to the non-ordered SAM. Two kinds of trisaccharides receptors terminating in sialic acid-α2,6- galactose (6′-sialyllactose) and in sialic acid-α2,3-galactose (3′-sialyllactose) were conjugated directly with the SiO_2 surface of FET devices by a glycoblotting method. The FETs with densely immobilized glycans, which possess the high capture ability by achieving the glycoside cluster effect, clearly distinguish HA molecules between their subtypes H1 (human) and H5 (avian) at attomolar level, while the conventional method based on HA antibodies achieves only picomolar level detection. Fig. 7a shows a schematic representation of the glycan-modified FET-based biosensor and Fig. 7b shows the glycoblotting method.

2.5. Passivation, gate dielectric and noise

ImmunoFET technology seems as a natural extension to the well-established silicon-based MOSFET industry. However, one important distinction between an immunoFET and a conventional MOSFET is the working environment; while MOSFET operates in ambient conditions, immunoFET is expected to perform in a solution environment. Therefore, the passivation of the immunoFET metal lines is of a considerable importance and challenge. SiO_2 and Si_3N_4 have been widely used for device passivation in silicon-based immunoFETs as they provide satisfactory protection against moisture and ambient solution (Choi et al., 2012; Kim et al., 2012a; Shalev et al., 2013). The hydrophobicity or hydrophilicity of the passivation materials is an important property and can significantly affect the sensor's performance. Kim et al. reported to achieve enhanced sensitivity simply by changing the surface property of the passivation layers which covers the interconnecting metal lines except the active area (Kim et al., 2013). Two

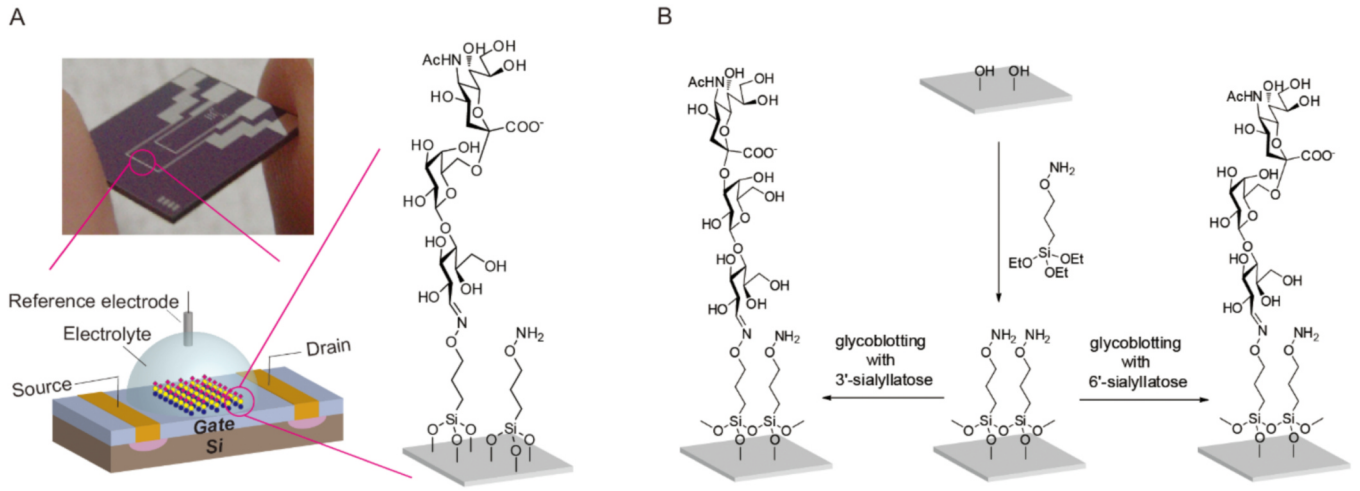

Fig. 7. Glycan-immobilized field effect transistor (FET) biosensor. (A) Optical image of an FET chip and schematic illustration of glycan-immobilized FET for highly sensitive and specific detection of influenza virus hemagglutinin (HA). (B) One step functionalization of the SiO2 surface of FET devices with aminooxy terminated trialkoxysilane reagent followed by glycoblotting with unmodified glycans. Copied from Hideshima et al. (2013b). Copyright © 2013, American Chemical Society.

types of passivation layers, Si_3N_4 for the hydrophilicity and CYTOP™ (Asahi glass company, Japan) for the hydrophobicity, were used for a controlled comparison. The hydrophobic passivation surface increased the binding probability of biomolecules by confining the biomolecules inside the designed hydrophilic sensing region and the sensitivity is reported to improve more than 100-fold for CYTOP-Si_3N_4 passivation compared to that with Si_3N_4 passivation only.

Moreover, the gate oxide of the immunoFET serves three purposes: a) protect the channel from degradation by the solution, b) generate Ψ_0 following the Nernst equation, and c) generate the field-effect property for signal amplification (Abe et al., 1979). For the past few decades, the use of SiO_2 in CMOS technology has been encouraged due to its robust nature and the industry accumulated knowledge of oxide process control. However, SiO_2 gate dielectrics suffer from issues such as band offset, interfacial structure, boron penetration and reliability (Wilk et al., 2001). Due to its high water resistance, Si_3N_4 has often been used with SiO_2 for long-term stability and to minimize gate leakage current (Ma, 1998). Al_2O_3, a high dielectric material, has also been extensively used as stacked gate oxide due to its excellent chemical stability in physiological environments and high immunity to hysteresis (Bae et al., 2013; Bousse et al., 1990; Jang and Cho, 2013; Peled et al., 2014; Yong et al., 2012; Zhou et al., 2014). Ta_2O_5 has been reported to possess high surface buffer capacity which helps to achieve better sensitivity (Bobrov et al., 1991; Kwon et al., 1996; Lue et al., 2011). Other high-κ materials like HfO_2, TiO_2, Y_2O_3 have also been studied (Chou and Liao, 2004; Pan and Liao, 2007; Zafar et al., 2011). Rare-earth oxides have also been rigorously investigated as potential replacement of SiO_2 (Pan and Lin, 2010; Pan and Huang, 2011; Pan et al., 2009). However, the biggest problem of rare-earth oxides is moisture absorption due to oxygen vacancies which effects their sensing performance (Zhao et al., 2006). To overcome this issue, elements like Ti or Y are added to the rare-earth oxide films (Pan and Lin, 2010; Pan et al., 2010; Wu et al., 2010). Pan et al. investigated the effect of yttrium content on the structural properties and sensing characteristics of YbY_xO_y sensing membranes for electrolyte-insulator-semiconductor (EIS) sensors for label-free detection of rheumatoid factor (Pan et al., 2015).

As devices are scaled down to the nanometer regime, the channel current becomes more prone to fluctuations due to fluctuations of the inversion charge near the Si–SiO_2 interface. This arises from the variations of the interfacial oxide charge after dynamic trapping–detrapping of free carriers into slow oxide traps (which can affect carrier density, carrier mobility or both) (Ghibaudo and Boutchacha, 2002). Thus, low-frequency noise of the device becomes a very serious limitation for any DC measurement (Tsai and Ma, 1994). In immunoFETs, the noise from the electrochemical interface and the biological environment contribute additional complexity to the noise performance of the device. The EIS system consists of two electrochemical interfaces namely electrode-electrolyte interface and the electrolyte insulator interface. Noise at the electrode-electrolyte interface arises from the charge transfer across the bulk electrolyte (Deen et al., 2006). Hassibi et al. presented a comprehensive study of the noise processes in electrode-electrolyte systems and proposed a model composed of noise components due to the resistance at the interface and redox generated noise (Hassibi et al., 2004). They showed that when charge transfer occurs at the electrode-electrolyte interface, frequency dependent shot noise becomes apparent in addition to the thermal noise originating from all the dissipative components. The shot noise frequency spectrum is governed by the charge and mass transfer processes at the proximity of the interface such that if the mass transfer is dominated by electric field effects, the noise spectra possesses a $1/f^2$ dependency while in diffusion-dominant electrode, the excess noise due to ionic redistribution obeys inverse frequency power law (i.e. $1/f$ noise).

Rajan et al. investigated the temperature-dependent $1/f$ noise mechanism in nanowire biochemical FETs from weak to strong inversion in a temperature range 100–300 K (Rajan et al., 2010). The primary effect due to the decrease in temperature is the reduction in the number of interface traps, which are thermally accessible. Thus at low temperatures, the correlated mobility fluctuations are suppressed and the $1/f$ noise is dominated by carrier number fluctuations, resulting in a Lorentzian spectrum. Deen et al. presented a complete circuit diagram of a bioFET with noise sources as shown in Fig. 8 (Deen et al., 2006). The noise sources V_1^2 and V_2^2 model the charge transfer resistance noise and the bulk electrolyte resistance noise, respectively. The noise source I_1^2 represents the noise due to the Faradaic process that can occur in the electrode-electrolyte interface. The noise source I_2^2 represents the combined effect of the thermal noise and the flicker noise of the FET's channel. The noise source V_3^2 represents an anticipated noise source due to the random motion of the immobilized DNA probes within the electrolyte. This motion can couple to the semiconductor channel and cause random fluctuations in the carriers. They considered the noise due to the electrolyte bulk resistance to be white noise, with the spectral density S_{VRb} described as:

$$S_{V_{R_b}} = 4kTR_b, \tag{25}$$

where R_b is the electrolyte bulk resistance. Thus, when the electrolyte

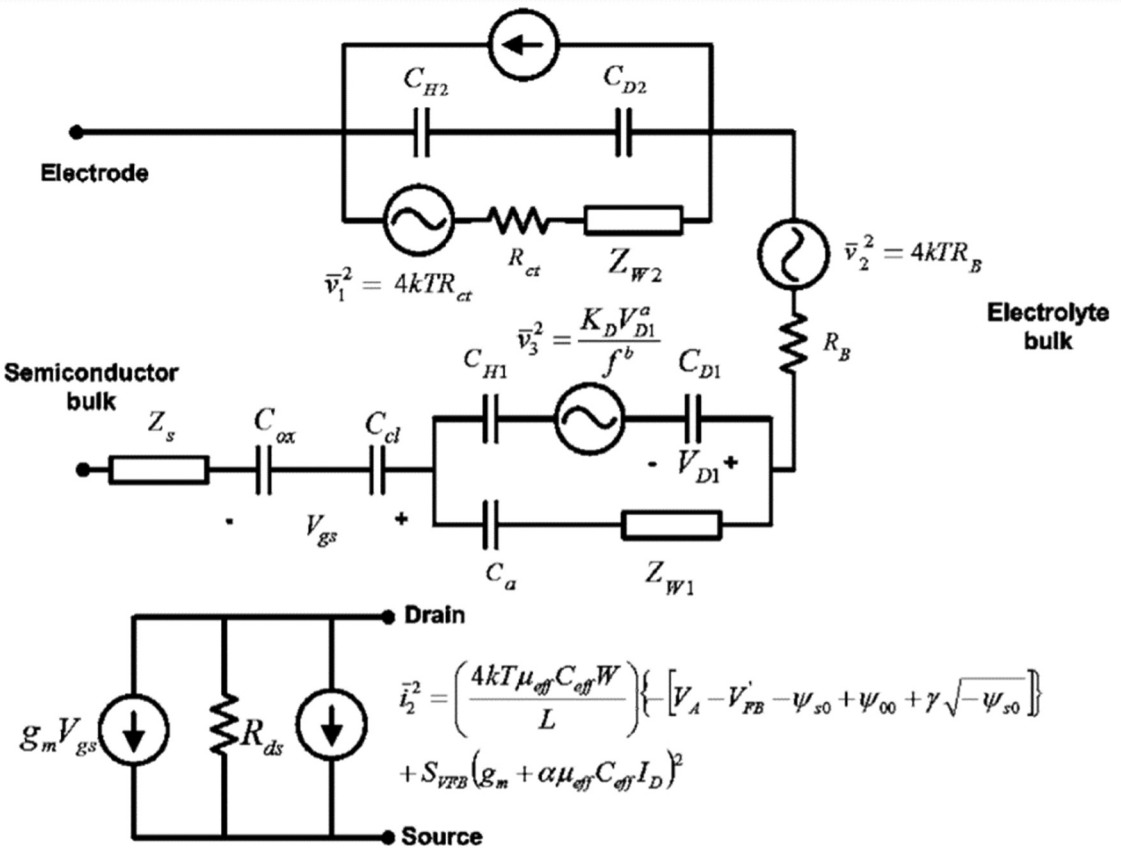

Fig. 8. Complete equivalent circuit model for the bioFET showing the various noise contributions. Copied from Deen et al. (2006). Rights managed by AIP publishing.

concentration increases, the electrolyte resistance decreases and according to Eq. (25), the noise from the electrolyte also decreases. Therefore, from the point of view of noise, it would be desirable to have a high electrolyte concentration to minimize the bulk resistance. However, for high enough electrolyte concentrations, the low-frequency noise of the FET dominates over the electrolyte noise, so the electrolyte concentration should be lowered to have high sensitivity (Deen et al., 2006).

Rajan et al. reported that signal-to-noise ratio (SNR) is an intrinsic device property and is maximized at the region of maximum transconductance (g_m) (Rajan et al., 2011). SNR can be used as a performance metric for designing better sensors since it involves both g_m as well as the drain current noise power density (SI) such that

$$SI = g_m^2 S_{Vg} = \left(1+\gamma\mu C_{ox}\frac{I_{DS}}{g_m}\right)^2 g_m^2 S_{VFB}, \tag{26}$$

where γ is Coulombic scattering coefficient, S_{Vg} is the power spectral density of the gate voltage noise and S_{VFB} is the flatband-voltage noise spectral density due to fluctuations in the interface/oxide charge which is given by

$$S_{VFB} = \frac{\lambda kTq^2 N_{ot}}{fWLC_{ox}^2}, \tag{27}$$

where λ is the tunneling parameter for electrons in silicon oxide ($\sim 10^{-10}$ m), N_{ot} is the oxide trap density and f is the frequency at which the power of the noise density is measured. Thus, the SNR of an immunoFET is given by (Rajan et al., 2014)

$$SNR = \frac{g_m}{\sqrt{SI}} = \sqrt{\frac{WLC_{ox}^2 f}{\lambda kTq^2 N_{ot}}}. \tag{28}$$

Wu et al. experimentally studied the noise characteristics of ultra-thin dual gate transistors and its effect on the intrinsic limit of detection of these transistors. Unlike single gate transistors, the response of DGFETs is amplified by an asymmetric factor governed by the capacitive coupling of the top and bottom oxides such that their response exceeds Nernst limit which is elaborately discussed in the later section. However, this capacitive signal amplification cannot be translated to proportional increase in the intrinsic LOD because the noise amplitude increases commensurate with the asymmetry factor, thus neutralizing the effect of capacitive amplification (Wu et al., 2017).

The effect of surface functionalization on device noise and performance have also been studied (Delker et al., 2013; Kim et al., 2012b). Rajan et al. investigated the effect of APTES functionalization on the noise properties of bioFETs and reported a 3-fold increase in SNR which indicate almost an order of magnitude decrease in the trap density (Rajan et al., 2014). Also, the SNR is directly proportional to $\sqrt{area}$ which means increasing the device area results in higher SNR. This contradicts the common argument that smaller devices have better sensitivity. Therefore, device size should be carefully determined based on the experimental requirements to optimize the SNR.

3. ImmunoFET for label-free detection: device architectures

Specificity, dynamic range and sensitivity coupled with device robustness and stability determine the performance vector for a sensing technology to become a viable option for applications in immunosensing. Although, in principle, immunoFETs are capable of real-time, specific and sensitive PPI detection, still there are several fundamental obstacles and challenges in the realization of commercial immunoFETs that are related to, for example, the operationality of a silicon device in liquid environment (e.g. device encapsulation and surface passivation of the active gate oxide area), Debye screening and the stability of the reference electrode. Structural modifications were proposed to circumvent these obstacles which led to the development of new and

Table 1
Recent reports on silicon-based immunoFETs applied to clinical diagnosis.

Analyte	Gate dielectric	Linker	Buffer	Response time	Dynamic range	LOD	Sensitivity	Reference
Cytokeratin fragment 21-1 (CYFRA 21-1)	SiO_2	APTES	0.01 × PBS	**	1 ng/mL to 1 μg/mL	1 ng/mL	10.8 ± 2.7 mV (ng/mL)$^{-1}$	(Cheng et al., 2015)
Neuron-specific enolase (NSE)						10 ng/mL	2.5 ± 2.1 mV (ng/mL)$^{-1}$	
α-feto protein (AFP)	SiO_2	APS	0.01 × PBS	**	100 pg/mL to 1 μg/mL	100 pg/mL	100 mV (μg/mL)$^{-1}$	(Cheng et al., 2014)
Antigen 85 complex B (Ag85B)	Si_3N_4	APTES	0.01 × PBS	Real time	0.12 μg/mL to 1 μg/mL	0.12 μg/mL	286.6 mV μg^{-1}	(Saengdee et al., 2016)
Hepatitis B surface antigens (HBsAg)	SnO_2	APTES	1 × PBS	**	22.5 fg/mL to 22.5 ng/mL	22.5 fg/mL	690.15 mV/dec	(Lee et al., 2015)
Influenza A Virus HemagglutininHuman (H1 HA)	SiO_2	AOPTES	0.01 × PBS	10 min	50 a.M. to 5 nM	50 a.M.	**	(Hideshima et al., 2013b)
Annexin A3 (ANXA3)	SnO_2	–	Artificial urine pH 10 buffer	20 min	0.1 fg/mL to 10 μg/mL	< 1 fg/mL	33.3 mV/dec	(Jeun et al., 2017)
Cardiac troponin (cTnI)	SiO_2	APTMS	0.01 × PBS	Real time	10 pg/mL to 10 μg/mL	10 pg/ml100 fg/mL	**	(Shalev et al., 2013)
Prostate specific antigen (PSA)								
Cardiac troponin I (cTnI)	ZnO-NPs	APTES	0.01 × PBS	10 min	1 ng/mL to 10 μg/mL	3.24 pg/mL	35.3 nA (g/mL)$^{-1}$	(Fathil et al., 2017)
Avian Influenza (AI)	SiO_2	–	1 × PBS	Real time	**	250 ng/mL	**	(Kim et al., 2012a)
Cortisol	SnO_2	PSMA	1 × PBS	**	10 fg/mL to 10 ng/mL	1 pg/mL	**	(Jang et al., 2018)
Immunoglobulin G (IgG)	SiO_2	APTMS	0.1 × MES	Real time	**	6.5 nM	40 mV/dec	(Shalev et al., 2012)
	Si_3N_4							

** Data not specified in the literature.

innovative device configurations. These configurations differ not only in their structure but also in the sensing mechanism and operational principles. Recently, Lowe et al. extensively reviewed bioFETs specifically used for streptavidin detection by surface-bound biotin, which are commonly used biological systems to emulate immunosensing (Lowe et al., 2017). This section discusses in detail the important silicon based immunoFETs in which label-free sensing was demonstrated excluding structures such as nanowires, nanobelts and nanoribbons as they have been already extensively review elsewhere (Chen et al., 2011b; Mu et al., 2015). Table 1 presents a summarized list of publications on silicon-based immunoFETs used for the detection of various analytes along with their sensitivities, dynamic range and limit of detection.

3.1. Basic immunoFET

In its most basic form, the immunoFET structure consists of an ISFET in which the gate dielectric is functionalized with ligands to detect the targeted analyte as shown in Fig. 1c. In the following, we briefly review several recent studies on silicon-based immunoFETs in terms of the strategies for surface chemical functionalization and gate dielectric material selection. Osaka's group demonstrated antibody-modified FET treated with bovine serum albumin (BSA) blocking for label-free immunosensing of tumor marker protein, α-fetoprotein in blood serum with a detection limit of 10 ng/mL. The SiO_2 surface was functionalized with 3-aminopropyl silane (APS) followed by GA. BSA blocking was used to minimize non-specific adsorption of other blood proteins (Hideshima et al., 2012). In a different work, they established antigen-binding fragment (Fab) immobilized immunoFET for the label-free detection of AFP for a concentration range of 100 pg/mL to 1 μg/mL in 0.01 × PBS. Fab receptors are the recognition and binding domains of antibodies. To examine the effect of the receptor's size, the responses of the Fab-immobilized and antibody-immobilized FETs in the presence of AFP were compared. The Fab immobilized FET showed a ΔV_T of 111 mV for 1 μg/mL of AFP, while the antibody-immobilized FET had a ΔV_T of 51 mV. The use of small Fab receptors allowed immunosensing within the Debye length and they reported enhanced sensitivity by lowering the LOD from 10 ng/mL to 100 pg/mL (Cheng et al., 2014). Recently, they demonstrated label-free immunosensing of PPI between lung tumor markers cytokeratin fragment 21-1 (CYFRA21-1) and neuron-specific enolase (NSE) in both phosphate buffer solution (PBS) and human serum using multi-analyte SiO_2 gate dielectric p-type silicon immunoFET (Cheng et al., 2015). The SiO_2 gate oxide surface was modified with APTES SAM and the cross-linker GA. The non-specific adsorption of other proteins in human serum was minimized by using a blocking reagent BSA. Fig. 9a shows the change in V_T of the BSA-blocked immunoFET after the addition of a mixture of CYFRA21-1 and NSE in human serum. The limit of detection achieved for CYFRA21–1 and NSE in human serum was 1 ng/mL and 100 ng/mL, respectively. This difference between the sensitivity of the analytes was reported to be due to steric hindrance.

Saengdee et al. demonstrated label-free immunosensing of protein antigen 85 complex B (Ag85B) for tuberculosis diagnosis using silicon immunoFET (Saengdee et al., 2016). The Si_3N_4 sensing layer on the SiO_2 gate dielectric of an n-channel ISFET was modified with APTES followed by GA, yielding an aldehyde-terminated surface. They achieved a linear response for concentration between 0.12 and 1 μg/mL without significant interference from other recombinant proteins. Fig. 9b shows the high specificity of the Ag85B immunosensor for native Ag85B protein of *M. tuberculosis* with gate potential change response of 26.0 ± 2.6 mV. Fathil et al. proposed zinc oxide nanoparticles (ZnO-NPs) thin film based FET for the label-free sensing of cardiac troponin I (cTnI) (Fathil et al., 2017). They used ZnO-NPs thin film as the channel on p-type silicon-on-insulator (SOI) wafer to create p-n-p junction between the source, channel and drain. The surface of the thin film is functionalized with APTES followed by GA. Although the conducting channel is not sustained in silicon, still we acknowledge

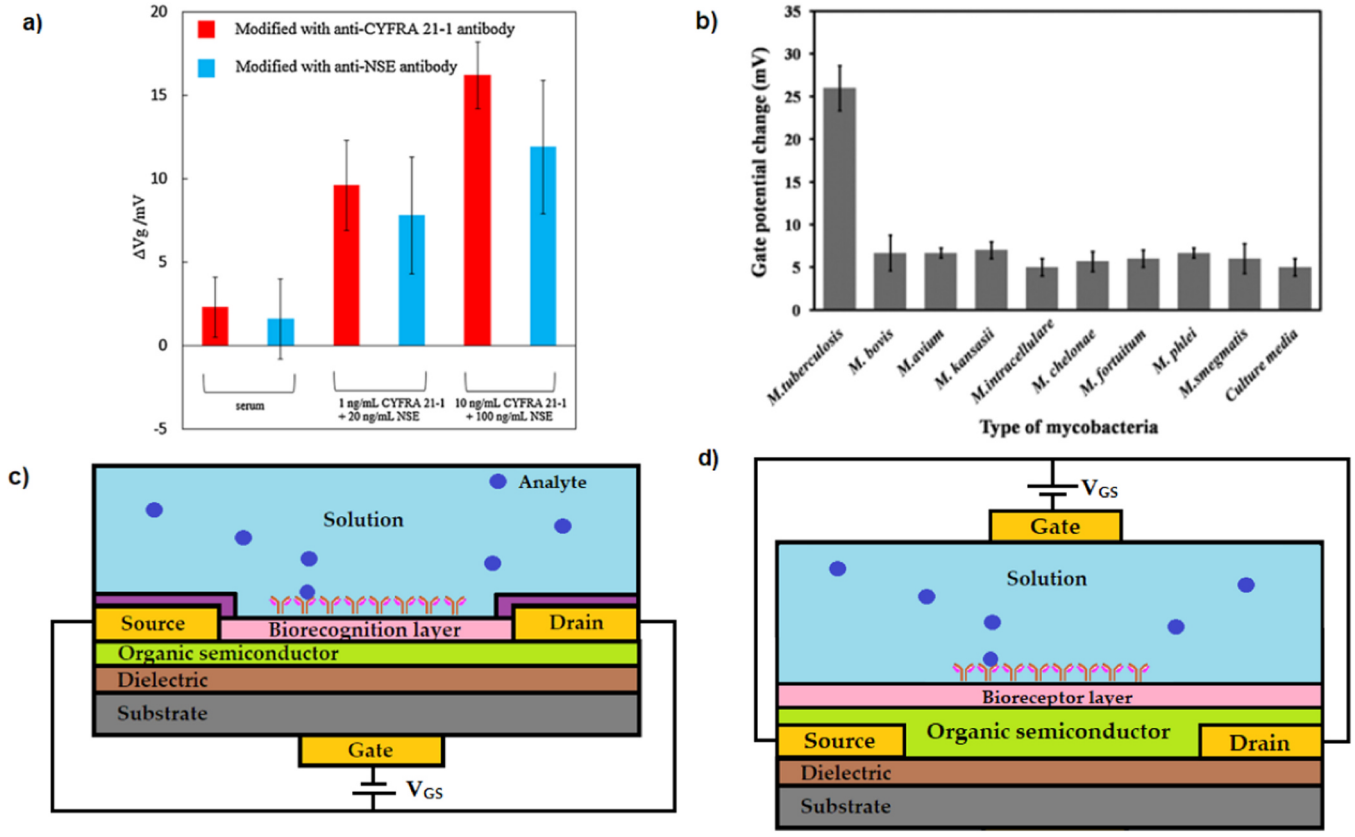

Fig. 9. a) The change in V_T for detection of multiple target proteins (a mixture of CYFRA 21-1 and NSE) at low concentrations in human serum using a BSA-blocked multianalyte FET biosensor. The error bars show the standard deviation (n = 5). Copied from Cheng et al. (2015). Copyright © 2015, Elsevier. **b)** The gate potential change (ΔV) corresponding to the native Ag85B protein of various mycobacteria species. Each data set displayed the average and standard deviation (SD) of the results obtained for three independent experiments (n = 3). Reprinted with permission from Saengdee et al. (2016). Copyright © 2016, Royal Society of Chemistry. **c),d)** Schematic representation of an organic FET and electrolyte-gated organic FET structure respectively. A bioreceptor layer (pink) is immobilized on the organic semiconductor layer (green) which is deposited on Si(grey)/SiO_2(brown) substrate. V_{GS} is the applied gate voltage. Adapted from Kergoat et al. (2012). (For interpretation of the references to color in this figure legend, the reader is referred to the web version of this article).

their contribution as they used the SOI substrate to manipulate the sensing performance; they demonstrated substrate-gate coupling in the FET by applying voltage biasing from the substrate of the SOI to improve the sensitivity by controlling conductivity of the channel. They measured a linear response of the relative change in drain current over logarithmic cTnI analyte concentration ranging from 1 ng/mL to 10 μg/mL with limit of detection of 3.24 pg/mL.

Recently, organic field effect transistors (OFETs) have received immense research interest and have emerged as a potential sensor platform for its numerous advantages such as high sensitivity, low cost, easy fabrication and mechanical flexibility, which has encouraged their utilization in a large number of applications. The OFET structure resembles the basic immunoFET structure where the silicon channel is replaced with an organic semiconductor and the gate is biased through the substrate as shown in Fig. 9c. Another configuration derived from the OFET is the electrolyte-gated OFET (EGOFET) in which the gate bias is applied to the electrolyte instead of the substrate as illustrated in Fig. 9d. Their structures and sensing mechanism have been extensively reviewed elsewhere so here we include only a few latest works which proposed label free immunodetection (Kergoat et al., 2012; Lee et al., 2017; Mei et al., 2013; Torsi et al., 2013). Katz and group demonstrated label free detection of glial fibrillary acidic protein using pentacene based OFET with polyethylene glycol containing bioreceptor layer for an analyte concentration range of 0.5–100 ng/mL and achieved LOD of 1 ng/mL (Song et al., 2017). In the following year, the same group experimentally studied the influence of the bioreceptor layer on the sensitivity of pentacene based OFET for label free detection of myelin basic protein. They achieved highest sensitivity of (11.9 ± 3.8)% for polystyrene-*co*-methacrylic acid (PS-MA) as a receptor layer since large amounts of antibodies was successfully immobilized on the device surface (Song et al., 2018). Jang et al. demonstrated acetylchloline (ACh^+) using 5,5′-bis-(7-dodecyl-9H-fl uoren-2-yl)-2,2′-bithiophene based OFET functionalized with perallyloxyCB[6] ($(allyloxy)_{12}CB[6]$, AOCB[6]) and achieved LOD of 1×10^{-12} M ACh^+ (Jang et al., 2015). Wustoni et al. demonstarted label free detection of human prion protein using thiamine immobilized silicon FET for a concentration range of 40 nM to 40 pM. They also reported improved sensitivity by dual-ligand binding achieved by the addition of metal ions (Cu^{+2}, Mn^{+2}, Zn^{+2}) which amplifies the FET response due to the effect of the association of the protein with the metal ions (Wustoni et al., 2014). Torsi and group demonstrated label free detection of C-reactive protein (CRP) using poly-3-hexylthiophen (P3HT) based EGOFET immunosensor in high ionic concentrations and showed capacitive sensing makes the FET response insensitive to Debye screening (Palazzo et al., 2015). In the following year, they demonstrated label free CRP detection using similar immunosensor for wide dynamic range from 4 pM to 2 μM with LOD of 2 pM (220 ng/mL) (Magliulo et al., 2016). Recently, the same group demonstrated label free detection of procalcitonin (PCT) for a concentration range of 0.8 pM to 4.7 nM with LOD of 2.2 pM using the same EGOFET immunosensor (Seshadri et al., 2018).

3.2. Floating gate ImmunoFET

Fig. 10a presents a schematic of a floating gate field effect transistor

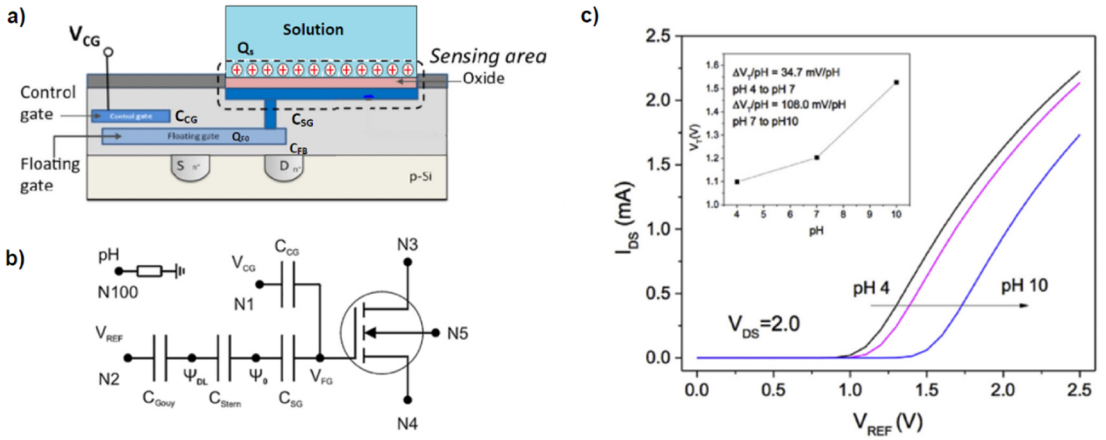

Fig. 10. a) Schematic representation of the floating gate immunoFET structure. The control gate, which is capacitively coupled with the floating gate, controls the conductivity of the semiconductor channel. The sensing mechanism of FGFET is potentiometric in which any variation in the bound charge Q_s on the active area causes a shift in the threshold voltage of the transistor. Adapted from Zhang et al., 2015. **b)** Macromodel description of the FGFET. The model input nodes: N1 is the CG potential (V_{CG} node), N2 is the REF potential (V_{REF} node), N3 is drain voltage (V_D node), N4 is the source voltage (V_S node), N5 is the body terminal of the transistor and N100 is defined as the pH input. The Gouy–Chapman–Stern model defines the capacitors of the double layer and the surface potential of the oxide Ψ_0 and the potential at the Stern layer Ψ_{DL}. Copied from Kaisti et al. (2017). Copyright © 2016, Elsevier. **c)** pH monitoring with polyaniline-functionalized ion-sensitive FGFET with inset showing the change in threshold voltage V_T with pH, $\Delta V_T/pH = 108\,mV/pH$ for pH 7–10. Copied from Zhang et al. (2018). Copyright © 2017, Elsevier.

(FGFET). Shen et al. introduced the chemoreceptive neuron MOS (CνMOS) based on FGFET for chemical and molecular sensing (Shen et al., 2003). The main attraction of this device was the elimination of the reference electrode. Instead, a control gate is utilized to control the channel conductivity. This provided a solution to the problem of integrating a reference electrode into a CMOS fabrication process which would increase the complexity of device fabrication and hence affect the realization of low-cost, disposable devices.

Barbaro et al. introduced a charge-modulated FET based on floating gate structure for DNA hybridization detection and presented a model to explain its working principle (Barbaro et al., 2006). In FGFET, a polysilicon floating gate (FG) layer is inserted between the control gate (CG) and the source/drain electrode pair such that the FG is capacitively coupled to CG on one end and is connected to the sensing area on the other as shown in Fig. 10a. The potential between the FG and the silicon body, V_{FG} can be expressed as:

$$V_{FG} = \frac{C_{CF}}{C_{CF} + C_{FB}} V_{CG} + \frac{Q_{F0} - Q_i(Q_s)}{C_{CF} + C_{FB}}, \tag{29}$$

where C_{CF} is the capacitance between the CG and the FG, C_{FB} is the capacitance between the FG and the silicon, Q_{F0} is the total charge trapped in the FG, Q_s is the bound active surface charge and Q_i is the charge induced on the FG surface by Q_s. So I_{DS} of the transistor indirectly depends on both the CG voltage and Q_s via V_{FG} as:

$$I_{DS} = \mu C_{ox} \frac{W}{L}((V_{FG} - V_T)V_{DS} - \frac{V_{DS}^2}{2}). \tag{30}$$

Any variation in the net charge on the active area due to biological binding will induce a corresponding change in V_T of the transistor which serves as an indicator of the biological detection. The relationship between the effective threshold voltage ($V_{T,eff}$) of the transistor and Q_s can be expressed as:

$$V_{T,eff} \cong V_T - \frac{Q_{F0} - Q_i(Q_s)}{C_{CF} + C_{FB}} \text{for} C_{CF} \gg C_{FB}. \tag{31}$$

However, the absence of the reference electrode may result in unstable electric measurement since the electrolyte is in a floating potential (Guan et al., 2013). Jayant et al. reported that the use of reference electrode along with the control gate can manipulate the biomolecule immobilization to enhance sensitivity by altering the electric field at the sensing oxide (Jayant et al., 2013). This electric-field modulation of the dielectric surface is termed as electrofluidic gating. Kaisti et al. proposed that the interplay between the CG and the reference electrode in an ion-sensitive FGFET can be used for electrofluidic gating i.e. control the charging of the sensor surface and ion screening layer via the field effect (Kaisti et al., 2017, 2015). Using the macro model illustrated in Fig. 10b, they described the device operation in which the change in V_{FG} of FGFET resulting from the inputs is given as

$$\Delta V_{FG} = \frac{C_{CG}}{C_{TOT}} \Delta V_{CG} + \frac{C_{SG}}{C_{TOT}} \Delta \Psi_0, \tag{32}$$

$$\Psi_0 = V_{cell}^0 + V_{REF} + V_{pH}, \tag{33}$$

where C_{SG} is the sensing gate capacitance per unit area, $C_{TOT} = C_{SG} + C_{CG} + C_{ox}$, V_{cell}^0 describes the constant interfacial potentials associated to the electrochemical cell and V_{pH} is the chemically relevant term. Chen et al. proposed folded FGFET topology in which the floating gate is placed above the control gate, covering the entire device such that the top device area can be utilized as the sensing area which is directly above the FET (Chen et al., 2011a). This allows sensing and detection at the same location on the chip. They tested the device for different poly amino acids and demonstrated reliable detection of charge fluctuations on the sensing area of the device. Since the sensing mechanism of the FGFET is potentiometric, the Debye length remains a challenging obstacle. To circumvent this problem, Zhang et al. proposed polyaniline functionalized ion sensitive FGFET and utilized the ion and redox sensitive nature of polyaniline for detection of pH and horseradish peroxidase (HRP) catalyzed enzymatic reactions on the sensing area. Fig. 10c shows the transfer characteristics recorded for pH 4–10 by adding 20 μL of each buffer to the PDMS well with an Ag/AgCl electrode inserted in the buffer. As the redox reactions occur very close to the polyaniline transducer layer, the EDL problem can be significantly reduced (Zhang et al., 2018). Although immunosensing based on silicon-FGFET is yet to be reported, we included this structure in our review as the cited works in DNA hybridization detection indicate its potential applications in immunosensing.

3.3. Extended gate ImmunoFET

The extended gate field-effect transistor (EGFET) was introduced in

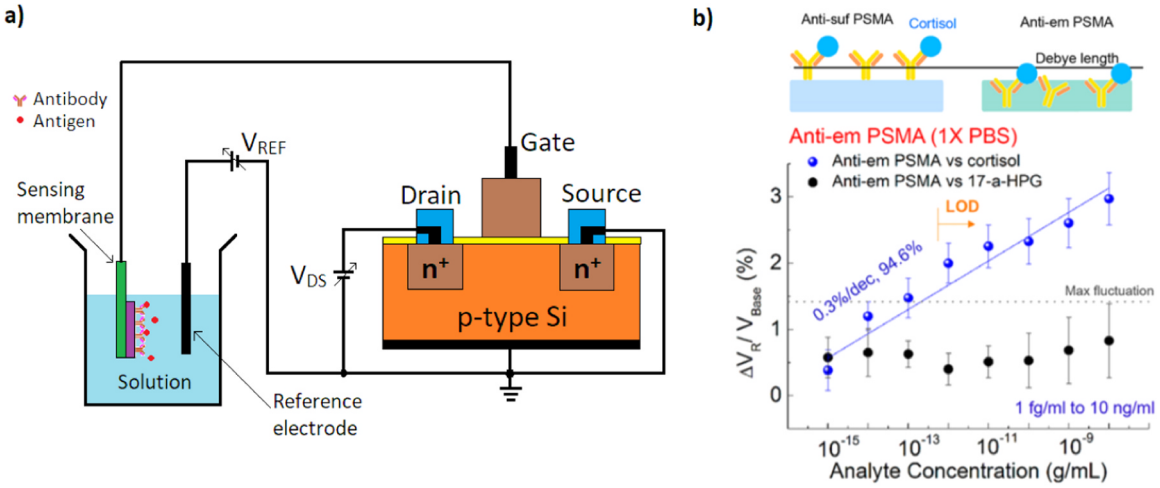

Fig. 11. a) An illustration of the extended-gate immunoFET. The sensing structure containing the sensing membrane is dipped into the solution with analytes. The gate of the transistor is connected to the sensing structure via an extended metal line. V_{DS} denotes the source-drain voltage and V_{REF} is the reference voltage. Adapted from Guliga et al. (2014). **b)** Schematic representation of an antibody embedded polymer (Anti-em PSMA) sensing structure used for cortisol detection. The graph shows the percentage change in responsive voltage $\Delta V_R/V_{base}$ of anti-em PSMA for varying cortisol and 17-α-HPG concentration. ΔV_R increases by 0.3% with increasing cortisol over eight samples of anti-em PSMA. Copied from Jang et al. (2018). Copyright © 2018, American Chemical Society.

1983 by van der Spiegel et al. as an improvement to the conventional ISFET in terms of passivation and packaging (van der spiegel et al., 1983). As shown in Fig. 11a, it consists of two parts, one is the sensing structure consisting of the sensing membrane that comes in contact with the solution and the other is the MOSFET structure. The gate of the MOSFET can be metallic such as gold or polysilicon which is directly connected to the sensing structure via metal. The removal of the FET structure from the biochemical liquid environment via an extended gate supported long term stability of the device as well as allowed flexibility in the design of the sensing area. Also, a wide variety of bioreceptors can be conveniently immobilized on the extended electrode to maximize amplification and provide ease of fabrication without affecting the semiconducting device. Moreover, the transistor can be tested and characterized separately without contacting the solution and the light and temperature effects can also be avoided (Chen et al., 2003). Thus, EGFETs have been intensively employed to design low-cost, disposable biosensors for clinical applications.

Guan et al. discussed a label-free potentiometric non-enzymatic sensor using off-chip EGFET with a ferrocenyl-alkanethiol modified gold electrode for determining the uric acid concentration in human serum and urine. The sensor detects the change in the interfacial potential which is determined by the redox state of the ferrocene compound on the gold electrode. They achieved a limit of detection of 500 nM and the sensor showed excellent long term reliability over a period of at least six months (Guan et al., 2014). Lin et al. investigated the use of aptamers for specific detection of platelet-derived growth factor (PDGF) and subsequently triggered the rolling circle amplification (RCA) of DNAs on EGFET to enhance sensitivity (Lin et al., 2016). The RCA primer immobilized on the sensing surface amplifies the protein signal into the elongation of DNAs, allowing the EGFET to achieve a detection limit of 8.8 pM in serum. Recently, Jang et al. proposed antibody embedded polymer on the sensing area as illustrated in Fig. 11b to overcome the problem of Debye screening. The sensing membrane was made by linking poly(styrene-*co*-methacrylic acid) (PSMA) with anticortisol before coating the modified polymer on the remote gate (Jang et al., 2018). As shown in Fig. 11b, they demonstrated sensitivity from 10 fg/mL to 10 ng/mL for cortisol using the antibody embedded receptor in the polymer and a limit of detection (LOD) of 1 pg/mL in 1 × PBS where Debye length λ_D is 0.2 nm. They also showed a LOD of 1 ng/mL in lightly buffered artificial sweat. Chen et al. proposed a portable urea biosensor based on EGFET using SnO_2/ITO glass as the sensing electrode (Chen et al., 2003). They demonstrated urea detection based on pH variation with a dynamic range of 0.31–120 mg/dl in 5 mM PBS and reported a response time of 1–2 min. Chi et al. proposed EGFET based on SnO_2 pH sensitive membrane on electrode connected to a commercial MOSFET device CD4007UB or LF356N and showed linear pH response of about 56–58 mV/pH in a concentration range of pH 2–12. They reported that EGFET reduced the effects from ambient light and showed that the reference voltage shifted only about 3 mV when exposed to 2000 lx light illumination (Chi et al., 2000). Kao et al. presented a multi-analyte biosensor on CF_4 plasma treated Nb_2O_5 sensing membrane with EGFET for urea and glucose sensing based on pH variation (Kao et al., 2014). They reported that CF_4 plasma treatment reduced dangling bonds and passivated defects by forming strong bonds and showed that for urea and glucose, the sensitivity increased from 2.61 mV/mM and 5.62 mV/mM respectively for as-deposited membrane to 7.71 mV/mM and 10.59 mV/mM respectively for CF_4 plasma treated sensing membrane. Lin et al. presented an EGFET assembled with a microfluidic chip and achieved sensitivity of 37.45 mV/mM for measuring hydrogen ions at pH 6–8 with a linearity of 0.9939, 7 mV/mM for measuring glucose with a linearity of 0.9962, and 8.01 mV/mM for measuring urea with a linearity of 0.9809. Additionally, for Apolipoprotein A1 (APOA1) detection, they used magnetic beads combined with DNA fragments as labeling to detect protein concentration without modifying the sensor surface with antibody in advance and reported minimum detection limit of approximately 12.5 ng/mL (Lin et al., 2015). Various other groups also demonstrated labeled immunosensing using EGFETs (Kamahori et al., 2007; Seong et al., 2018).

3.4. Double gate ImmunoFET

Double gate field-effect transistor (DGFET) is based on SOI technology. Fig. 12a presents the DGFET structure which consists of the active SOI layer sandwiched between a top gate (and the corresponding thin front gate dielectric) and a bottom gate (with a corresponding comparatively thicker back gate dielectric). The dependence of the top gate threshold voltage on the bottom gate voltage has been elaborately discussed by Lim and Fossum, in which they demonstrated that for sufficiently thin SOI ($t_{Si} < kW_{max}$ for $1 < k < 2$), complete depletion of the channel occurs (referred to as fully-depleted (FD) SOI) which results in the coupling of the two gates such that the threshold voltage of one gate becomes dependent on the surface potential of the other gate (Colinge, 1988; Lim and Fossum, 1983). The SOI thickness

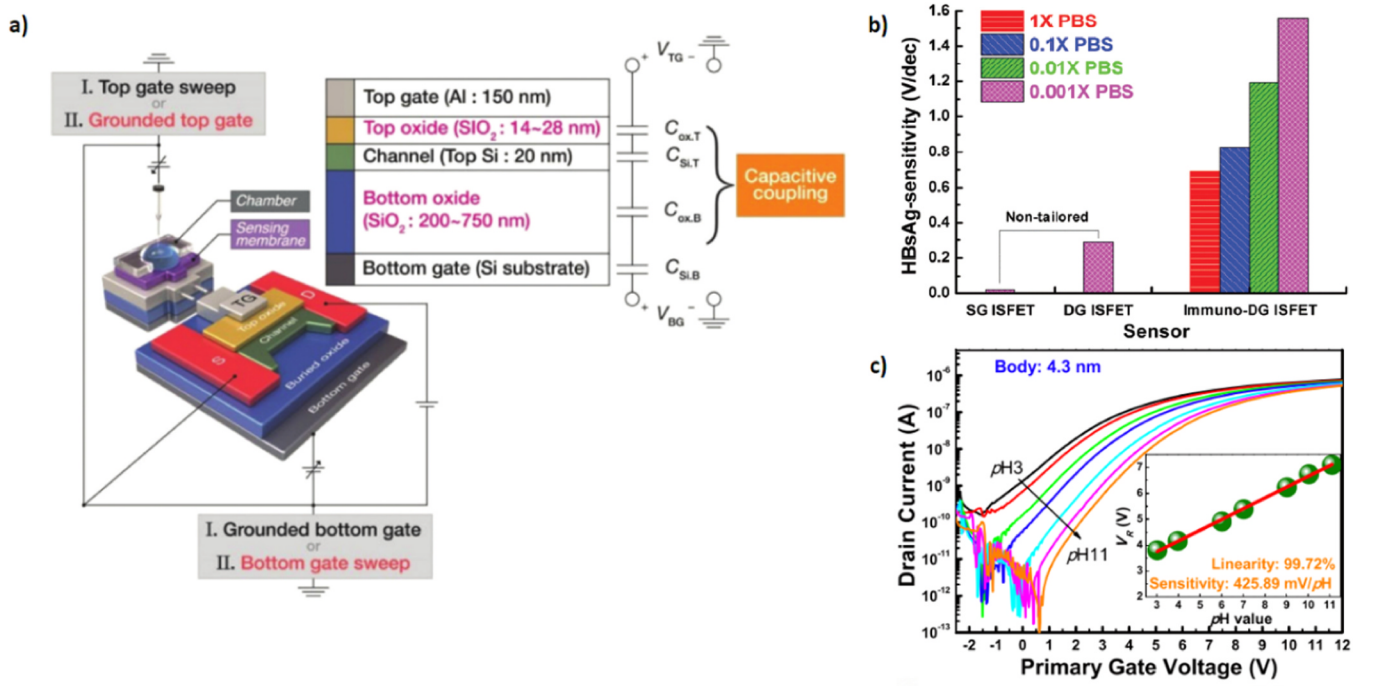

Fig. 12. a) A schematic diagram of the double gate immunoFET sensor (DGFET). The DGFET structure consists of a bottom gate and a top gate with the semiconductor layer sandwiched between them. For a fully depleted SOI, the top gate becomes capacitively coupled to the bottom gate. Reprinted with permission from Lee et al. (2015). Copyright © 2015, RSC pub. **b)** Hepatitis B surface antigen (HBsAg) sensitivity depending on different ionic strength of PBS in tailored DG ISFET and comparison with HBs sensitivities in other sensors. Reprinted with permission from Lee et al. (2015). Copyright © 2015, RSC pub. **c)** Transfer curves of 4.3 nm ultra-thin SOI based DG ISFET for various pH buffer solutions. The inset shows the response voltage curve with high linearity 99.72% and sensitivity 425.89 mV/pH. Copied from Jang and Cho (2014). Copyright © 2014, Springer Nature.

determines the nature of the coupling between the bottom and top gates. This dependence is shown as (Jang and Cho, 2014)

$$\Delta V_{th}^{b} = \frac{3t_{ox}^{b}}{t_{Si} + 3t_{ox}^{t}} \Delta V_{th}^{t}, \tag{34}$$

where $t_{ox}{}^{b}$, $t_{ox}{}^{t}$ and t_{Si} are the thicknesses of the bottom gate oxide, top gate oxide and the SOI, respectively. Thick body introduces non-ideal factors such as unstable capacitive coupling ratio and leakage components that degrade the DGFET performance. Dual gate operation has been studied with the aim to develop highly sensitive biosensors capable of exceeding the Nernst limit. Jang et al. reported enhanced pH sensitivity of 425.89 mV/pH with linearity of 99.72% for 4.3 nm ultra-thin SOI DGFET as illustrated in Fig. 12c (Jang and Cho, 2014).

In a conventional ISFET, the shift in the top-gate threshold voltage ($V_T{}^{t}$) caused by the shift in Ψ_0 is given as

$$\Delta V_T^{t} = -\Delta\Psi_0, \tag{35}$$

whereas in FD SOI dual-gate structure and depleted top interface, the effect of the top gate on the bottom gate threshold voltage ($V_T{}^{b}$) can be shown as (Jang and Cho, 2012):

$$\Delta V_T^{b} = \frac{C_{top}}{C_{bottom}} \Delta V_{th}^{t} = -\frac{C_{top}}{C_{bottom}} \Delta\Psi_0, \tag{36}$$

where C_{top} and C_{bottom} are the top and bottom gate dielectric capacitances per unit area, respectively. Therefore, in comparison with conventional ISFETs, the threshold voltage shifts due to changes in the top interface potential is enhanced by capacitive coupling factor of C_{top}/C_{bottom}. Cho's group reported a significantly enhanced pH sensitivity of 379.2 mV/pH for FD SOI based DGFET (Jang and Cho, 2012). In a different work, they reported improved sensing performance of polycrystalline silicon-based DGFET with pH sensitivity of 325.8 mV/pH using $SiO_2/HfO_2/Al_2O_3$ (OHA) sensing layer which also significantly reinforced the chemical stability and sensing margin of the device (Jang et al., 2012). Shalev et al. reported label free and specific detection of 6.5 nM immunoglobulin G (IgG) with 40 mV shift in the threshold voltage with pH sensitivity of 35 mV/decade (Shalev et al., 2012). Lee et al. reported the detection of Hepatitis B surface antigen using immuno-DGFET and achieved detection limit of 22.5 fg/mL in non-diluted 1 × PBS medium with high sensitivity of 690 mV as shown in Fig. 12b (Lee et al., 2015). Recently, Wu et al. experimentally studied the effect of capacitive amplification on the sensor detection limit using sub-10 nm ultrathin silicon FETs. They reported that the noise amplitude in DGFET increases in proportion to the ratio of the asymmetric top and bottom oxides and thus neutralizes the capacitive signal amplification such that the intrinsic LOD of single and double gate FETs become comparable (Wu et al., 2017). Moreover, in FD SOI based FET, instability factors like hysteresis and drift effects have been reported to slightly increase in dual gate operation as compared to that of single gate mode of operation (Jang and Cho, 2012).

Khamaisi et al. demonstrated an enhancement-mode FD SOI FET based biosensor for the detection of surface immobilized-biotin and streptavidin (gate oxide was functionalized with (3-aminopropyl) trimethoxysilane (APTMS)) (Khamaisi et al., 2010). They reported that the pH sensitivity of the sensor decreased after the formation of APTMS and biotin layer but slightly increased after the binding of streptavidin due to the large amount of amine and carboxylic side chains on the protein. They also studied the effects of the charge and dipole of these organic layers by monitoring the threshold voltage of the bottom gate of the device. Moreover, they reported a reduction in the channel gain following the formation of each of the organic layers due to their dielectric nature which changes the effective capacitance of the system. Jeun et al. demonstrated the detection of annexin A3 (ANXA3), a biomarker for prostate cancer using dual-gate FET based ion-responsive urine sensor (IRUS) with a disposable sensing gate and proposed a self-normalized detection method by measuring reference signals from each patient's urine sample (Jeun et al., 2017). They achieved a good linearity of 96.15% for a dynamic range of 0.1 fg/mL to 10 μg/mL, a high

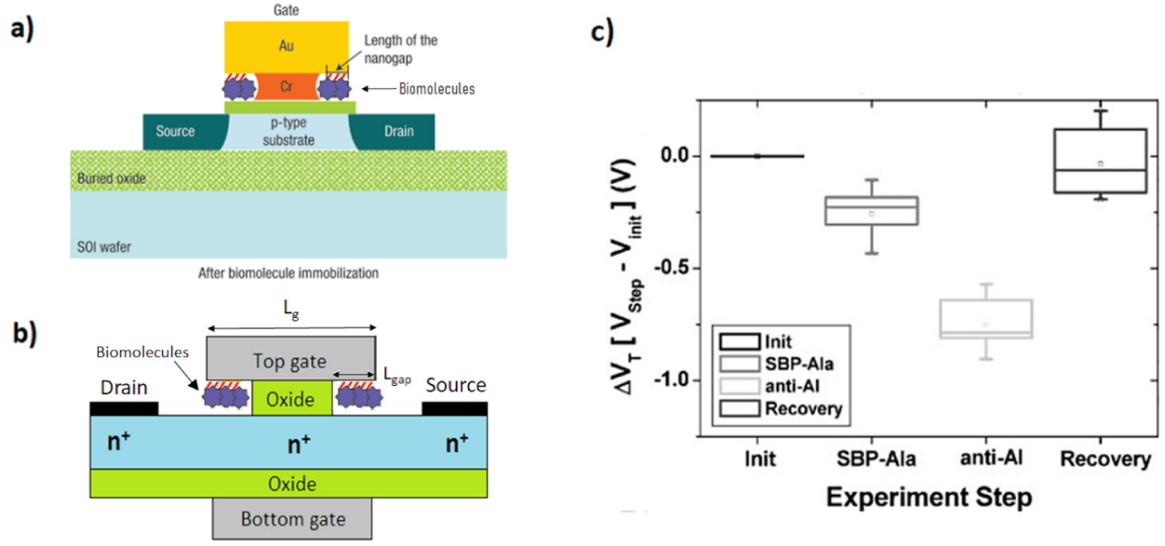

Fig. 13. a) A schematic representation of the DMFET showing the silicon body (blue), the gate oxide (green) and the chromium (orange) and gold (yellow) electrodes. The chromium layer is partially etched to form an air gap that can be filled with biomolecules. Copied from Im et al. (2007). Copyright © 2007, Springer Nature. **b)** A schematic representation of a junctionless double-gate DMFET. L_g and L_{gap} are the gate length and nanogap length respectively. Adapted from Parihar and Kranti (2015). **c)** Change in threshold voltage (ΔV_T) after immobilization of SBP–AIa, binding of anti-AI, and recovery by detaching SBP–AIa and anti-AI. Copied from Gu et al. (2009). Copyright © 2009, John Wiley and Sons.(For interpretation of the references to color in this figure legend, the reader is referred to the web version of this article).

sensitivity of 33.3 mV/dec and LOD smaller than 1 fg/mL.

3.5. Dielectric modulated ImmunoFET

Dielectric modulated field-effect transistor (DMFET) based on SOI with a 15 nm nanogap in the gate oxide (Fig. 13a) was first experimentally demonstrated for PPI biosensing by Choi's group (Im et al., 2007). They observed a significant V_T shift of ~0.8V due to the change in the effective dielectric constant of the gate oxide following the label-free and specific binding of streptavidin to the immobilized-biotin in the nanogap. Label-free detection of avian influenza antigen (AIa) using silicon binding proteins (SBP) for a fixed concentration of 25 μg/mL was also demonstrated for a 20 nm nanogap (Fig. 13c) (Gu et al., 2009). The DMFET was later developed into a nanogap-embedded separated DGFET in a 6 × 6 array configuration for point-of-care testing and demonstrated label-free detection of AI using SBP-AIa and anti-AI immobilization (Im et al., 2011). In another work, they investigated the surface potential distribution of the DMFET and derived an analytical model of the V_T shift of the transistor from the potential model (Choi et al., 2010). The proposed model also provided useful guidelines for optimization of the nanogap dimensions to maximize sensitivity (ΔV_T). The concept of capacitive sensing by dielectric modulation enabled the label-free detection of neutral biomolecules with high sensitivity.

The threshold voltage V_T of a DMFET is given as (Kim et al., 2008)

$$V_T = V_{FB} + 2\phi_B + \frac{Q_B}{C_{DMFET}} - \frac{Q_{ox}}{C_{DMFET}} \tag{37}$$

$$\frac{1}{C_{DMFET}} = \frac{1}{C_{mole}} + \frac{1}{C_{ox}} + \frac{1}{C_{air}} = \frac{T_{mole}}{k_{mole}\varepsilon_0} + \frac{T_{ox}}{k_{ox}\varepsilon_0} + \frac{T_{air}}{\varepsilon_0}, \tag{38}$$

where V_{FB} is the flatband voltage, ϕ_B is the surface band bending, C_{DMFET} is the total capacitance of the gate dielectric materials in the DMFET, C_{mole} and C_{air} indicate the capacitances of the biomolecule and air respectively, T_{mole}, T_{air}, *and* T_{ox} denote the thickness of the biomolecule, air and silicon dioxide respectively and k_{mole} *and* k_{ox} are the matching dielectric constants of the biomolecule and silicon dioxide respectively. Kranti's group numerically investigated the performance of cavity based dielectric modulated double-gate junctionless transistor (JL-DG-DMFET) as illustrated in Fig. 13b. They reported that the occurrence of impact ionization in JL-DG-DMFET improves the detection sensitivity of the sensor which can be utilized for biosensing applications (Parihar and Kranti, 2015). They demonstrated significant V_T shift even for partially filled cavity (20% fill-in factor) by using asymmetric biasing mode. Recently, they experimentally investigated the operation of DMFET biosensor architecture based on tunneling (TFET) and accumulation mode FET (AMFET) for label-free detection of iris protein (Dwivedi and Kranti, 2018). They reported that both TFET and AMFET suffer from antigen location dependent sensitivity degradation. TFET exhibits high sensitivity when antigens are close to the tunneling junction but their performance and applicability are severely limited when antigens move away from the tunneling junction. AMFET exhibits higher sensitivity when antigen layer is located close to the center of the cavity and its sensitivity degrades as antigen layer shifts towards the extreme ends of the cavity. However, they reported better performance of AMFET compared to that of TFET for biosensing applications. Rahman et al. presented an analytical model to investigate the effect of antigen position and the cavity fill-in factor on the JL-DG-DMFET sensitivity for label-free detection (for various antigens like proteins, enzymes, cells and DNA etc.). They reported that maximum sensitivity is achieved for completely filled cavity, and for partially filled cavity the sensitivity is enhanced by moving the antigens toward the center of the channel and away from the drain (Rahman et al., 2017).

Various groups also demonstrated label-free DNA detection using DMFET and presented different structures and operation modes as briefly reviewed in the following. Kim et al. experimentally studied the effect of charge on the DMFET operation by introducing neutralized as well as negatively charged DNA in the nanogap. They reported that n-channel DMFET can preferably detect neutral or positively charged biomolecules whereas p-channel DMFET showed better sensitivity for negatively charged biomolecules (Kim et al., 2008). Narang et al. proposed a dielectric modulated double-gate tunnel FET (DG-TFET) based on p-i-n and p-n-p-n structures for label-free DNA detection and numerically analyzed its application for the detection of charged, neutral and hybridized biomolecules (Narang et al., 2012). They reported that the p-n-p-n structure based TFET biosensor exhibited higher sensitivity compared to that of a MOSFET in terms of on-current (I_{on}), off-current (I_{off}) and V_T along with added advantages of low leakage current and steep subthreshold swing. Kalra et al. numerically investigated the

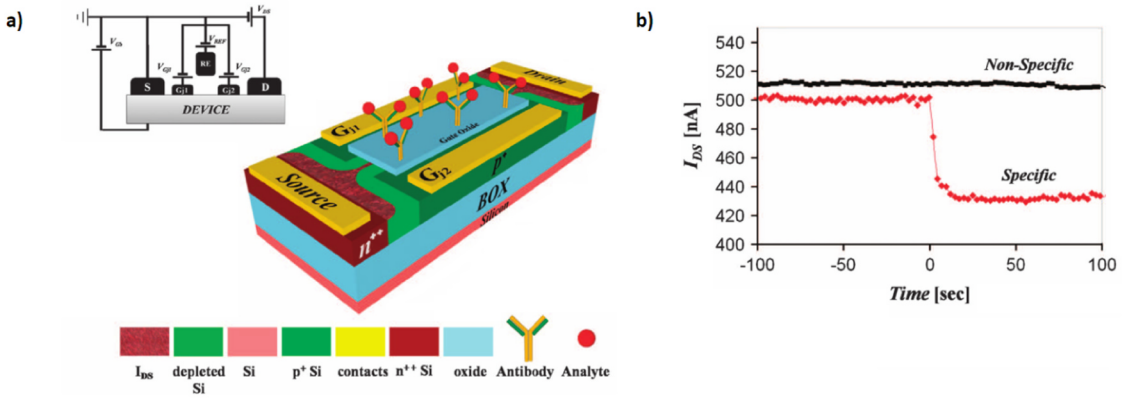

Fig. 14. a) Schematic illustration of the EFN biosensor with antibody/analyte complexes bonded to the gate dielectric. **b)** I_{DS} response to injection of 10 pg/mL cTnI at t = 0 s. Non-specificity is also demonstrated because no change in current is apparent following injection of 10 pg/mL of cTnI to a device modified solely with APTMS (at t = 0 s). Copied from Shalev et al. (2013). Copyright © 2013, Springer Nature.

performance of DMFET for DNA detection and reported that the orientation of the DNA in the nanogap governs the sensitivity and dominance of charge or dielectric constant effect in nanogap embedded FET devices. They demonstrated that vertical DNA orientation in p-channel DMFET leads to higher sensitivity compared to n-channel DMFET biosensors (Kalra et al., 2016).

3.6. Electrostatically formed nanowire

ImmunoFET based on the electrostatically formed nanowires (EFN) was first proposed by Shalev et al. for label-free, specific and real-time detection of femtomolar protein concentrations (Shalev et al., 2013). The EFN biosensor consists of an accumulation-type planar transistor surrounded by four gates: a back gate, a front gate and two lateral gates as shown in Fig. 14a. The nanoscale-conducting channel is not physically fabricated but is induced and controlled by the depletion regions formed by the four surrounding gates. The electrostatic control of the nanowire-like conducting channel allows EFN biosensor fabrication using standard integrated circuit processes and eliminates the need for sophisticated fabrication tools and techniques.

The EFN is conceptually different from the conventional silicon nanowire (SiNW). The confinement of current in SiNW is compositional, i.e. it is due to the material (for example, air or SiO_2) with different properties surrounding the wire. On the other hand, the confinement is fully electrostatic in the EFN device; that is, it is due to the external applied bias. Thus, EFN allows the flexibility to determine the size and shape of the channel as well as its lateral and z-locations post-fabrication unlike the SiNWs in which these parameters remain predetermined and fixed. Furthermore, the EFN is inherently immune to performance degradation observed in bottom-up growth methods (i.e. e.g. due to diffusion of metal catalysts into the conducting channel (Koren et al., 2011b, 2011a)) as EFN is realized using conventional standard top-down silicon fabrication techniques. Additionally, the signal-to-noise ratio of EFNs can be improved by removing the conducting channel sufficiently away from the Si/SiO_2 interface which is a dominant source of low-frequency noise as discussed earlier.

Shalev et al. reported that the sensitivity of the EFN is governed by the electrostatic downscaling of the sensor active area to dimensions comparable to that of the target analytes. They demonstrated real-time, specific and label-free detection of cardiac troponin (cTnI) and prostate specific antigen (PSA) concentrations as low as 10 pg/mL (~340 fM) and 100 fg/mL (~3 fM) respectively in 0.01 × phosphate-buffered saline buffer solution at pH 7. The shift in $V_T{}^t$ is given by

$$\Delta V_T^t = -\frac{Q_{analyte}}{C_{analyte}} = -\frac{Q^*_{analyte} \bullet t^2_{analyte}}{\varepsilon_{analyte}}, \quad (39)$$

where $Q_{analyte}$, $Q^*_{analyte}$, $C_{analyte}$, $\varepsilon_{analyte}$ and $t_{analyte}$ are the overall charge, the charge density per unit volume (i.e. the analyte charge density directly above the conducting nanowire), the capacitance, the permittivity and the thickness of the analyte layer, respectively. Fig. 14b shows the drain current response following the binding of cTnI due to the shift in the threshold voltage. A 15% decrease in I_{DS} is clearly observed following the cTnI binding at t = 0 s.

4. Conclusions

In the past few years, highly sensitive, label-free and specific detection of various antigen-antibody interactions have been demonstrated using silicon-based immunoFETs. Silicon-based immunoFETs allow for label-free and real-time detection, ultra-high sensitivity and superb LOD, excellent selectivity, the possibility for multiplexing, support low sample volumes and CMOS compatibility. Despite the apparent simplicity of the immunoFET, the commercialization of such technologies is yet to be demonstrated. The main hurdle for the realization of a product-based immunoFET is the solid/solution interface which is a multi-parameter system that introduces substantial complexity to the device. We believe the key to the next advancement in immunoFET technology is to further develop an appropriate management strategy of the solid/solution interface.

In this review, the operating principles, challenges concerning Debye screening, surface functionalization, device encapsulation, noise and performance limitations of silicon based immunoFETs have been summarized. Recent demonstrations of immunosensing using different immunoFET structures to overcome the design issues and achieve better performance have been highlighted. However, significant progress in the development of these biosensors at a commercial level is yet to be witnessed.

CRediT authorship contribution statement

Ie Mei Bhattacharyya: Data curation, Formal analysis, Writing - original draft. **Shira Cohen:** Data curation, Formal analysis, Writing - original draft. **Awad Shalabny:** Data curation, Formal analysis, Writing - original draft. **Muhammad Bashouti:** Conceptualization, Supervision, Writing - review & editing. **Barak Akabayov:** Conceptualization, Supervision, Writing - review & editing. **Gil Shalev:** Conceptualization, Supervision, Writing - review & editing.

Conflict of interest

The authors declare no conflict of interest.

Declaration of interests

None.

References

Abe, H., Esashi, M., Matsuo, T., 1979. ISFET's using inorganic gate thin films. IEEE Trans. Electron Devices 26, 1939–1944. https://doi.org/10.1109/T-ED.1979.19799.

Bae, T., Jang, H., Yang, J., Cho, W., 2013. High performance of silicon nanowire-based biosensors using a high - k stacked sensing thin film. Appl. Mater. Interfaces. https://doi.org/10.1021/am401026z.

Barbaro, M., Bonfiglio, A., Raffo, L., 2006. A charge-modulated FET for detection of biomolecular processes: conception, modeling, and simulation. IEEE Trans. Electron Devices 53, 158–166. https://doi.org/10.1109/TED.2005.860659.

Bard, A.J., Faulkner, L.R., 2001. Electrochemical methods fundamentals and applications. Mol. Biol. https://doi.org/10.1016/B978-0-08-098353-0.00003-8.

Bashouti, M.Y., Tung, R.T., Haick, H., 2009. Tuning the electrical properties of Si nanowire field-effect transistors by molecular engineering. Small 5, 2761–2769. https://doi.org/10.1002/smll.200901402.

Bergveld, P., 2003. ISFET, Theory and Practice, In: IEEE Sensor Conference Toronto. pp. 1–26.

Bergveld, P., 1970. Short communications: development of an ion-sensitive solid-state device for neurophysiological measurements. IEEE Trans. Biomed. Eng. https://doi.org/10.1109/TBME.1970.4502688.

Bobrov, P.V., Tarantov, Y.A., Krause, S., Moritz, W., 1991. Chemical sensitivity of an ISFET with Ta2O5 membrane in strong acid and alkaline solutions. Sens. Actuators B Chem. 3, 75–81. https://doi.org/10.1016/0925-4005(91)85010-G.

Boder, E.T., Midelfort, K.S., Wittrup, K.D., 2000. Directed evolution of antibody fragments with monovalent femtomolar antigen-binding affinity. PNAS 97, 10701–10705. https://doi.org/10.1073/pnas.170297297.

Bousse, L., Van Den Vlekkert, H.H., De Rooij, N.F.,, 1990. Hysteresis in A1203 -gate ISFETs. Sens. Actuators B 2, 103–110.

Broeck, H.C. Van Den, Cordewener, J.H.G., Nessen, M.A., America, A.H.P., Meer, I.M. Van Der, 2015. Label free targeted detection and quantification of celiac disease immunogenic epitopes by mass spectrometry. J. Chromatogr. A 1391, 60–71. https://doi.org/10.1016/j.chroma.2015.02.070.

Chan, K., Chung, C.Y., Yam, V.W., 2016. Parallel folding topology-selective label-free detection and monitoring of conformational and topological changes of different G-quadruplex DNAs by emission spectral changes via FRET of mPPE-Ala – Pt (II) complex ensemble. Chem. Sci. 2842–2855. https://doi.org/10.1039/c5sc04563k.

Chang, W., Yang, Y., Lu, H., Li, I., Liau, I., 2010. Spatio-temporal Characterization of Phagocytic NADPH Oxidase and Oxidative Destruction of Intraphagosomal Organisms 1–8.

Chen, B., Parashar, A., Pandey, S., 2011a. Folded floating-gate CMOS biosensor for the detection of charged biochemical molecules. IEEE Sens. J. 11, 2906–2910. https://doi.org/10.1109/JSEN.2011.2149514.

Chen, K.I., Li, B.R., Chen, Y.T., 2011b. Silicon nanowire field-effect transistor-based biosensors for biomedical diagnosis and cellular recording investigation. Nano Today 6, 131–154. https://doi.org/10.1016/j.nantod.2011.02.001.

Chen, J.C., Chou, J.C., Sun, T.P., Hsiung, S.K., 2003. Portable urea biosensor based on the extended-gate field effect transistor. Sens. Actuators B Chem. 91, 180–186. https://doi.org/10.1016/S0925-4005(03)00161-8.

Cheng, S., Hideshima, S., Kuroiwa, S., Nakanishi, T., Osaka, T., 2015. Label-free detection of tumor markers using field effect transistor (FET)-based biosensors for lung cancer diagnosis. Sens. Actuators B Chem. 212, 329–334. https://doi.org/10.1016/j.snb.2015.02.038.

Cheng, S., Hotani, K., Hideshima, S., Kuroiwa, S., Nakanishi, T., Hashimoto, M., Mori, Y., Osaka, T., 2014. Field effect transistor biosensor using antigen binding fragment for detecting tumor marker in human serum. Materials (Basel) 7, 2490–2500. https://doi.org/10.3390/ma7042490.

Chi, L.L., Chou, J.C., Chung, W.Y., Sun, T.P., Hsiung, S.K., 2000. Study on extended gate field effect transistor with tin oxide sensing membrane. Mater. Chem. Phys. 63, 19–23. https://doi.org/10.1016/S0254-0584(99)00184-4.

Choi, J.M., Han, J.W., Choi, S.J., Choi, Y.K., 2010. Analytical modeling of a nanogap-embedded FET for application as a biosensor. IEEE Trans. Electron Devices 57, 3477–3484. https://doi.org/10.1109/TED.2010.2076152.

Choi, K., Kim, J.Y., Ahn, J.H., Choi, J.M., Im, M., Choi, Y.K., 2012. Integration of field effect transistor-based biosensors with a digital microfluidic device for a lab-on-a-chip application. Lab Chip 12, 1533–1539. https://doi.org/10.1039/c2lc21203j.

Chou, J.C., Liao, L.P., 2004. Study of TiO2 thin films for ion sensitive field effect transistor application with RF sputtering deposition. Jpn. J. Appl. Phys. https://doi.org/10.1143/JJAP.43.61.

Chu, C.H., Sarangadharan, I., Regmi, A., Chen, Y.W., Hsu, C.P., Chang, W.H., Lee, G.Y., Chyi, J.I., Chen, C.C., Shiesh, S.C., Lee, G., Bin, Wang, Y.L., 2017. Beyond the Debye length in high ionic strength solution: direct protein detection with field-effect transistors (FETs) in human serum. Sci. Rep. 7, 1–15. https://doi.org/10.1038/s41598-017-05426-6.

Colinge, J.P., 1988. Thin-film SOI devices: a perspective. Microelectron. Eng. 8, 127–147. https://doi.org/10.1016/0167-9317(88)90013-5.

David, J., Jackson, 1999. Classical Electrodynamics. Wiley, New York.

Deen, M.J., Shinwari, M.W., Ranuárez, J.C., Landheer, D., 2006. Noise considerations in field-effect biosensors. J. Appl. Phys. 100. https://doi.org/10.1063/1.2355542.

Delker, C.J., Zi, Y., Yang, C., Janes, D.B., 2013. Low-frequency noise contributions from channel and contacts in InAs nanowire transistors. IEEE Trans. Electron Devices 60, 2900–2905. https://doi.org/10.1109/TED.2013.2274009.

Dwivedi, P., Kranti, A., 2018. Dielectric modulated biosensor architecture: tunneling or accumulation based transistor? IEEE Sens. J. 18, 3228–3235. https://doi.org/10.1109/JSEN.2018.2808948.

Engvall, E., 1980. Enzyme immunoawsay ELISA and EMIT. Methods Enzym. 70, 419.

Engvall, E., Perlmann, P., 1971. Enzyme-linked immunosorbent assay (ELISA) quantitative assay of immunoglobulin G. Immunochemistry 8, 871–874. https://doi.org/10.1016/0019-2791(71)90454-X.

Fathil, M.F.M., Md Arshad, M.K., Ruslinda, A.R., Gopinath, S.C.B., Nuzaihan, M.M.N., Adzhri, R., Hashim, U., Lam, H.Y., 2017. Substrate-gate coupling in ZnO-FET biosensor for cardiac troponin I detection. Sens. Actuators B Chem. 242, 1142–1154. https://doi.org/10.1016/j.snb.2016.09.131.

Friguet, B., Chaffotte, A.F., Djavadi-ohaniance, L., Goldberg, M.E., 1985. Measurements of the true affinity constant in solution of antige-antibody complexes by Enzyme-linked immunosorbent assay. J. Immunol. Methods 77, 305–319. https://doi.org/10.1016/0022-1759(85)90044-4.

Ghibaudo, G., Boutchacha, T., 2002. Electrical noise and RTS fluctuations in advanced CMOS devices. Microelectron. Reliab. 42, 573–582. https://doi.org/10.1016/S0026-2714(02)00025-2.

Goda, T., Miyahara, Y., 2013. Label-free and reagent-less protein biosensing using aptamer-modified extended-gate field-effect transistors. Biosens. Bioelectron. 45, 89–94. https://doi.org/10.1016/j.bios.2013.01.053.

Gotoh, M., Suzuki, M., Kubo, I., Tamiya, E., Karube, I., 1989. IMMUNO-FET sensor. J. Mol. Catal. 53, 285–292.

Gu, B., Park, T.J., Ahn, J.-H., Huang, X.-J., Lee, S.Y., Choi, Y.-K., 2009. Nanogap field-effect transistor biosensors for electrical detection of avian influenza. Small 5, 2407–2412. https://doi.org/10.1002/smll.200900450.

Guan, W., Duan, X., Reed, M.A., 2014. Highly specific and sensitive non-enzymatic determination of uric acid in serum and urine by extended gate field effect transistor sensors. Biosens. Bioelectron. 51, 225–231. https://doi.org/10.1016/j.bios.2013.07.061.

Guan, W., Rajan, N.K., Duan, X., Reed, M.A., 2013. Quantitative probing of surface charges at dielectric-electrolyte interfaces. Lab Chip 13, 1431–1436. https://doi.org/10.1039/c3lc41351a.

Guliga, H., Abdullah, W.F.H., Herman, S.H., 2014. Extended gate field effect transistor (EGFET) integrated readout interfacing circuit for pH sensing, In: 2014 Proceedings of the 2nd International Conference on Electrical, Electronics and System Engineering, ICEESE 2014. pp. 11–14. https://doi.org/10.1109/ICEESE.2014.7154605.

Haick, H., Ambrico, M., Ligonzo, T., Tung, R.T., Cahen, D., 2006. Controlling semiconductor/metal junction barriers by incomplete, nonideal molecular monolayers. J. Am. Chem. Soc. 128, 6854–6869. https://doi.org/10.1021/ja058224a.

Hassibi, A., Navid, R., Dutton, R.W., Lee, T.H., 2004. Comprehensive study of noise processes in electrode electrolyte interfaces. J. Appl. Phys. 96, 1074–1082. https://doi.org/10.1063/1.1755429.

Hideshima, S., Hinou, H., Ebihara, D., Sato, R., Kuroiwa, S., Nakanishi, T., Nishimura, S.-I., Osaka, T., 2013a. Attomolar Detection of Influenza A Virus Hemagglutinin Human H1 and Avian H5 Using Glycan-Blotted Field Effect Transistor Biosensor. Anal. Chem. 85, 5641–5644. https://doi.org/10.1021/ac401085c.

Hideshima, S., Kuroiwa, S., Kimura, M., Cheng, S., Osaka, T., 2013b. Effect of the size of receptor in allergy detection using field effect transistor biosensor. Electrochim. Acta 110, 146–151. https://doi.org/10.1016/j.electacta.2013.07.113.

Hideshima, S., Sato, R., Inoue, S., Kuroiwa, S., Osaka, T., 2012. Detection of tumor marker in blood serum using antibody-modified field effect transistor with optimized BSA blocking. Sens. Actuators B Chem. 161, 146–150. https://doi.org/10.1016/j.snb.2011.10.001.

Hierlemann, A., Baltes, H., 2003. CMOS-based chemical microsensors. Analyst 128, 15–28. https://doi.org/10.1007/978-3-540-33655-6_11.

Horowitz, G., 1998. Organic field-effect transistors. Adv. Mater. 10, 365–377. https://doi.org/10.1002/(sici)1521-4095(199803)10:5<365::aid-adma365>3.0.co;2-u.

Im, H., Huang, X.J., Gu, B., Choi, Y.K., 2007. A dielectric-modulated field-effect transistor for biosensing. Nat. Nanotechnol. 2, 430–434. https://doi.org/10.1038/nnano.2007.180.

Im, M., Ahn, J.H., Han, J.W., Park, T.J., Lee, S.Y., Choi, Y.K., 2011. Development of a point-of-care testing platform with a nanogap-embedded separated double-gate field effect transistor array and its readout system for detection of avian influenza. IEEE Sens. J. 11, 351–360. https://doi.org/10.1109/JSEN.2010.2062502.

Israelachvili, J., 1991. Intermolecular and Surface Forces, 2nd ed. Academic Press, London.

Jang, H., Cho, W., 2013. High performance silicon-on-insulator based ion-sensitive field-effect transistor using high-k stacked oxide sensing membrane. Appl. Phys. Lett. 043703, 1–4. https://doi.org/10.1063/1.3619831.

Jang, H.J., Bae, T.E., Cho, W.J., 2012. Improved sensing performance of polycrystalline-silicon based dual-gate ion-sensitive field-effect transistors using high-k stacking engineered sensing membrane. Appl. Phys. Lett. 100. https://doi.org/10.1063/1.4729762.

Jang, H.J., Cho, W.J., 2014. Performance enhancement of capacitive-coupling dual-gate ion-sensitive field-effect transistor in ultra-thin-body. Sci. Rep. 4, 1–8. https://doi.org/10.1038/srep05284.

Jang, H.J., Cho, W.J., 2012. Fabrication of high-performance fully depleted silicon-on-insulator based dual-gate ion-sensitive field-effect transistor beyond the Nernstian limit. Appl. Phys. Lett. 100. https://doi.org/10.1063/1.3685497.

Jang, H.J., Lee, T., Song, J., Russell, L., Li, H., Dailey, J., Searson, P.C., Katz, H.E., 2018. Electronic cortisol detection using an antibody-embedded polymer coupled to a field-effect transistor. ACS Appl. Mater. Interfaces 10, 16233–16237. https://doi.org/10.1021/acsami.7b18855.

Jang, M., Kim, H., Lee, S., Kim, H.W., Khedkar, J.K., Rhee, Y.M., Hwang, I., Kim, K., Oh, J.H., 2015. Highly sensitive and selective biosensors based on organic transistors functionalized with Cucurbit[6]uril derivatives. Adv. Funct. Mater. 25, 4882–4888. https://doi.org/10.1002/adfm.201501587.

Jayant, K., Auluck, K., Funke, M., Anwar, S., Phelps, J.B., Gordon, P.H., Rajwade, S.R., Kan, E.C., 2013. Programmable ion-sensitive transistor interfaces. II. Biomolecular sensing and manipulation. Phys. Rev. E 88, 1–11. https://doi.org/10.1103/PhysRevE.88.012801.

Jeun, M., Park, S., Kim, Y., Choi, J., Song, S.H., Jeong, I.G., Kim, C.S., Lee, K.H., 2017. Self-normalized detection of ANXA3 from untreated urine of prostate cancer patients without digital rectal examination. Adv. Healthc. Mater. 6, 1–7. https://doi.org/10.1002/adhm.201700449.

Jia, C.P., Zhong, X.Q., Hua, B., Liu, M.Y., Jing, F.X., Lou, X.H., Yao, S.H., Xiang, J.Q., Jin, Q.H., Zhao, J.L., 2009. Nano-ELISA for highly sensitive protein detection. Biosens. Bioelectron. 24, 2836–2841. https://doi.org/10.1016/j.bios.2009.02.024.

Jin, H., Yi, M., Young, C., Ahn, J., Gyu, H., Choi, C., Ha, S., Jung, T., Pil, J., 2017. High sensitive and selective electrochemical biosensor: label-free detection of human norovirus using affinity peptide as molecular binder. Biosens. Bioelectron. 87, 164–170. https://doi.org/10.1016/j.bios.2016.08.031.

Kaisti, M., Zhang, Q., Levon, K., 2017. Compact model and design considerations of an ion-sensitive floating gate FET. Sens. Actuators B Chem. 241, 321–326. https://doi.org/10.1016/j.snb.2016.10.051.

Kaisti, M., Zhang, Q., Prabhu, A., Lehmusvuori, A., Rahman, A., Levon, K., 2015. An ion-sensitive floating gate FET model: operating principles and electrofluidic gating. IEEE Trans. Electron Devices 62, 2628–2635. https://doi.org/10.1109/TED.2015.2441878.

Kalra, S., Kumar, M.J., Dhawan, A., 2016. Dielectric-modulated field effect transistors for DNA detection: impact of DNA orientation. IEEE Electron Device Lett. 37, 1485–1488. https://doi.org/10.1109/LED.2016.2613110.

Kamahori, M., Ishige, Y., Shimoda, M., 2007. A novel enzyme immunoassay based on potentiometric measurement of molecular adsorption events by an extended-gate field-effect transistor sensor. Biosens. Bioelectron. 22, 3080–3085. https://doi.org/10.1016/j.bios.2007.01.011.

Kao, C.H., Chen, H., Kuo, L.T., Wang, J.C., Chen, Y.T., Chu, Y.C., Chen, C.Y., Lai, C.S., Chang, S.W., Chang, C.W., 2014. Multi-analyte biosensors on a CF4plasma treated Nb2O5-based membrane with an extended gate field effect transistor structure. Sens. Actuators B Chem. 194, 419–426. https://doi.org/10.1016/j.snb.2013.12.056.

Kergoat, L., Piro, B., Berggren, M., Horowitz, G., Pham, M.C., 2012. Advances in organic transistor-based biosensors: from organic electrochemical transistors to electrolyte-gated organic field-effect transistors. Anal. Bioanal. Chem. 402, 1813–1826. https://doi.org/10.1007/s00216-011-5363-y.

Khamaisi, B., Vaknin, O., Shaya, O., Ashkenasy, N., 2010. Electrical performance of silicon-on- insulator field-effect transistors with multiple top-gate organic layers in electrolyte solution. ACS Nano 4, 4601–4608.

Kim, C., Jung, C., Park, H.G., Choi, Y., 2008. Novel dielectric-modulated field-effect transistor for label-free DNA detection. Biochip 2, 127–134 (https://doi.org/0000-0002-9447-3807).

Kim, J.Y., Choi, K., Moon, D., Il, Ahn, J.H., Park, T.J., Lee, S.Y., Choi, Y.K., 2013. Surface engineering for enhancement of sensitivity in an underlap-FET biosensor by control of wettability. Biosens. Bioelectron. 41, 867–870. https://doi.org/10.1016/j.bios.2012.08.036.

Kim, J.Y., Ahn, J.H., Choi, S.J., Im, M., Kim, S., Duarte, J.P., Kim, C.H., Park, T.J., Lee, S.Y., Choi, Y.K., 2012b. An underlap channel-embedded field-effect transistor for biosensor application in watery and dry environment. IEEE Trans. Nanotechnol. 11, 390–394. https://doi.org/10.1109/TNANO.2011.2175006.

Kim, S., Carpenter, P.D., Jean, R.K., Chen, H., Zhou, C., Ju, S., Janes, D.B., 2012b. Role of self-assembled monolayer passivation in electrical transport properties and flicker noise of nanowire transistors. ACS Nano 6, 7352–7361. https://doi.org/10.1021/nn302484c.

Koren, E., Elias, G., Boag, A., Hemesath, E.R., Lauhon, L.J., Rosenwaks, Y., 2011a. Direct measurement of individual deep traps in single silicon nanowires. Nano Lett. 11, 2499–2502. https://doi.org/10.1021/nl201019b.

Koren, E., Hyun, J.K., Givan, U., Hemesath, E.R., Lauhon, L.J., Rosenwaks, Y., 2011b. Obtaining uniform dopant distributions in VLS-grown Si nanowires. Nano Lett. 11, 183–187. https://doi.org/10.1021/nl103363c.

Kronik, L., Shapira, Y., 1999. Surface photovoltage phenomena: theory, experiment, and application. Surf. Sci. Rep. 37, 1–206.

Kwon, D.-H., Cho, B.-W., Kim, Ch-S., Sohn, B.-K., 1996. Effects of heat treatment on Ta205 sensing membrane for low drift and high sensitivity pH-ISFET. Sens. Actuators B 34, 441–445.

Landheer, D., Aers, G., McKinnon, W.R., Deen, M.J., Ranuarez, J.C., 2005. Model for the field effect from layers of biological macromolecules on the gates of metal-oxide-semiconductor transistors. J. Appl. Phys. 98. https://doi.org/10.1063/1.2008354.

Lee, I.K., Jeun, M., Jang, H.J., Cho, W.J., Lee, K.H., 2015. A self-amplified transistor immunosensor under dual gate operation: highly sensitive detection of hepatitis B surface antigen. Nanoscale 7, 16789–16797. https://doi.org/10.1039/c5nr03146j.

Lee, Y.H., Jang, M., Lee, M.Y., Kweon, O.Y., Oh, J.H., 2017. Flexible Field-Effect Transistor-Type Sensors Based on Conjugated Molecules. Chem 3, 724–763. https://doi.org/10.1016/j.chempr.2017.10.005.

Li, X., Song, S., Shuai, Q., Pei, Y., Aastrup, T., Pei, Y., Pei, Z., 2015. Real-time and label-free analysis of binding thermodynamics of carbohydrate-protein interactions on unfixed cancer cell surfaces using a QCM biosensor. Nat. Publ. Gr. 1–9. https://doi.org/10.1038/srep14066.

Lim, H.K., Fossum, J.G., 1983. Threshold Voltage of Thin-Film Silicon-on-Insulator. IEEE ELectron Device Lett. 30, 1244–1251.

Lin, M.Y., Hsu, W.Y., Yang, Y.S., Huang, J.W., Chung, Y.L., Chen, H., 2016. Immobilized rolling circle amplification on extended-gate field-effect transistors with integrated readout circuits for early detection of platelet-derived growth factor. Anal. Bioanal. Chem. 408, 4785–4797. https://doi.org/10.1007/s00216-016-9568-y.

Lin, Y.H., Chu, C.P., Lin, C.F., Liao, H.H., Tsai, H.H., Juang, Y.Z., 2015. Extended-gate field-effect transistor packed in micro channel for glucose, urea and protein biomarker detection. Biomed. Microdevices 17, 1–9. https://doi.org/10.1007/s10544-015-0020-4.

Lowe, B.M., Sun, K., Zeimpekis, I., Skylaris, C.K., Green, N.G., 2017. Field-effect sensors-from pH sensing to biosensing: sensitivity enhancement using streptavidin-biotin as a model system. Analyst 142, 4173–4200. https://doi.org/10.1039/c7an00455a.

Lue, C., Yu, T., Yang, C., Pijanowska, D.G., Lai, C., Park, H.T., 2011. Optimization of Urea-EnFET based on Ta2O5 layer with post annealing. Sensors 4562–4571. https://doi.org/10.3390/s110504562.

Ma, T.P., 1998. Making silicon nitride film a viable gate dielectric. IEEE Trans. Electron Devices 45, 680–690. https://doi.org/10.1109/16.661229.

Magliulo, M., De Tullio, D., Vikholm-Lundin, I., Albers, W.M., Munter, T., Manoli, K., Palazzo, G., Torsi, L., 2016. Label-free C-reactive protein electronic detection with an electrolyte-gated organic field-effect transistor-based immunosensor. Anal. Bioanal. Chem. 408, 3943–3952. https://doi.org/10.1007/s00216-016-9502-3.

Mei, J., Diao, Y., Appleton, A.L., Fang, L., Bao, Z., 2013. Integrated materials design of organic semiconductors for field-effect transistors. J. Am. Chem. Soc. 135, 6724–6746. https://doi.org/10.1021/ja400881n.

Mousavi, M.Z., Chen, H., Hou, H., Chang, C., Roffler, S., Wei, P., Cheng, J., 2015. Label-free detection of rare cell in human blood using gold nano slit surface plasmon resonance. Biosensors (Basel) 98–117. https://doi.org/10.3390/bios5010098.

Mu, L., Chang, Y., Sawtelle, S.D., Wipf, M., Duan, X., Reed, M.A., 2015. Silicon nanowire field-effect transistors—a versatile class of potentiometric nanobiosensors. IEEE Access 3, 287–302. https://doi.org/10.1109/ACCESS.2015.2422842.

Nair, P.R., Alam, M.A., 2010. Theory of "selectivity" of label-free nanobiosensors: a geometro-physical perspective. J. Appl. Phys. 107, 1–6. https://doi.org/10.1063/1.3310531.

Narang, R., Saxena, M., Gupta, R.S., Gupta, M., 2012. Dielectric modulated tunnel field-effect transistor-a biomolecule sensor. IEEE Electron Device Lett. 33, 266–268. https://doi.org/10.1109/LED.2011.2174024.

Natan, A., Kronik, L., Haick, H., Tung, R.T., 2007. Electrostatic properties of ideal and non-ideal polar organic monolayers: implications for electronic devices. Adv. Mater. 19, 4103–4117. https://doi.org/10.1002/adma.200701681.

Niwa, D., Omichi, K., Motohashi, N., Homma, T., Osaka, T., 2005. Organosilane self-assembled monolayer-modified field effect transistors for on-chip ion and biomolecule sensing. Sens. Actuators B Chem. 108, 721–726. https://doi.org/10.1016/j.snb.2004.11.055.

Pachauri, V., Ingebrandt, S., 2016. Biologically sensitive field-effect transistors: from ISFETs to NanoFETs. Essays Biochem. 60, 81–90. https://doi.org/10.1042/EBC20150009.

Palazzo, G., De Tullio, D., Magliulo, M., Mallardi, A., Intranuovo, F., Mulla, M.Y., Favia, P., Vikholm-Lundin, I., Torsi, L., 2015. Detection beyond Debye's length with an electrolyte-gated organic field-effect transistor. Adv. Mater. 27, 911–916. https://doi.org/10.1002/adma.201403541.

Pan, T.-M., Lin, C.-W., 2010. Structural and sensing characteristics of Dy2O3 and Dy2TiO5 electrolyte – insulator – semiconductor pH sensors. J. Phys. Chem. C 114, 17914–17919. https://doi.org/10.1021/jp107733u.

Pan, T., Huang, M., 2011. Structural properties and sensing characteristics of high-k Ho2O3 sensing film-based electrolyte – insulator – semiconductor. Mater. Chem. Phys. 129, 919–924. https://doi.org/10.1016/j.matchemphys.2011.05.032.

Pan, T., Liao, K., 2007. Influence of oxygen content on the structural and sensing characteristics of Y2O3 sensing membrane for pH-ISFET. Sens. Actuators B Chem. 128, 245–251. https://doi.org/10.1016/j.snb.2007.06.006.

Pan, T., Lin, T., Chen, C., 2015. Label-free detection of rheumatoid factor using YbY x O y electrolyte e insulator e semiconductor devices. Anal. Chim. Acta 891, 304–311. https://doi.org/10.1016/j.aca.2015.08.014.

Pan, T.M., Huang, M., De, Lin, C.W., Wu, M.H., 2010. Development of high-κ HoTiO3 sensing membrane for pH detection and glucose biosensing. Sens. Actuators B Chem. 144, 139–145. https://doi.org/10.1016/j.snb.2009.10.049.

Pan, T.M., Lin, J.C., Wu, M.H., Lai, C.S., 2009. Study of high-k Er2O3 thin layers as ISFET sensitive insulator surface for pH detection. Sens. Actuators B Chem. 138, 619–624. https://doi.org/10.1016/j.snb.2009.01.051.

Parihar, M.S., Kranti, A., 2015. Enhanced sensitivity of double gate junctionless transistor architecture for biosensing applications. Nanotechnology 26. https://doi.org/10.1088/0957-4484/26/14/145201.

Parizi, K.B., Xu, X., Pal, A., Hu, X., Wong, H.S.P., 2017. ISFET pH sensitivity: counter-ions Play a Key Role. Sci. Rep. 7, 1–10. https://doi.org/10.1038/srep41305.

Peled, A., Pevzner, A., Soroka, H.P., Patolsky, F., 2014. Morphological and chemical stability of silicon nanostructures and their molecular overlayers under physiological conditions: towards long-term implantable nanoelectronic biosensors. J. Nanobiotechnology 12, 1–11. https://doi.org/10.1186/1477-3155-12-7.

Pirincci, S.S., Ertekin, O., Laguna, D.E., Ozen, F.S., Ozturk, Z.Z., Ozturk, S., 2018. Label-free QCM immunosensor for the detection of ochratoxin A. Sensors 18. https://doi.org/10.3390/s18041161.

Rahman, E., Shadman, A., Khosru, Q.D.M., 2017. Effect of biomolecule position and fill in factor on sensitivity of a dielectric modulated double gate junctionless MOSFET biosensor. Sens. Bio-Sens. Res. 13, 49–54. https://doi.org/10.1016/j.sbsr.2017.02.002.

Rajan, N.K., Brower, K., Duan, X., Reed, M.A., 2014. Limit of detection of field effect transistor biosensors: Effects of surface modification and size dependence. Appl. Phys. Lett. 104. https://doi.org/10.1063/1.4867025.

Rajan, N.K., Routenberg, D.A., Chen, J., Reed, M.A., 2010. Temperature dependence of 1/

f noise mechanisms in silicon nanowire biochemical field effect transistors. Appl. Phys. Lett. 97, 2010–2013. https://doi.org/10.1063/1.3526382.
Rajan, N.K., Routenberg, D.A., Reed, M.A., 2011. Optimal signal-to-noise ratio for silicon nanowire biochemical sensors. Appl. Phys. Lett. 98, 1–4. https://doi.org/10.1063/1.3608155.
Reverberi, R., Reverberi, L., 2007. Factors affecting the antigen-antibody reaction. Blood Transfus. 5, 227–240. https://doi.org/10.2450/2007.0047-07.
Saengdee, P., Chaisriratanakul, W., Bunjongpru, W., Sripumkhai, W., Srisuwan, A., Hruanun, C., Poyai, A., Phunpae, P., Pata, S., Jeamsaksiri, W., Kasinreak, W., Promptmas, C., 2016. A silicon nitride ISFET based immunosensor for Ag85B detection of tuberculosis. Analyst 141, 5767–5775. https://doi.org/10.1039/c6an00568c.
Sakata, T., Kamahori, M., Miyahara, Y., 2005. DNA analysis chip based on field-effect transistors. Jpn. J. Appl. Phys. Part 1 Regul. Pap. Short. Notes Rev. Pap. 44, 2854–2859. https://doi.org/10.1143/JJAP.44.2854.
Sakata, T., Miyahara, Y., 2005. Detection of DNA recognition events using multi-well field effect devices. Biosens. Bioelectron. 21, 827–832. https://doi.org/10.1016/j.bios.2005.01.018.
Schenck, J.F., 1978. Theory, Design, and Biomedical Applications of Solid State Chemical Sensors. CRC Press Inc.
Seong, T.W., Seo, J., Lee, K.H., 2018. Full length histone H3 conjugated electrochemical biosensor for extracellular proteolytic Cathepsin L activity detection. Sens. Actuators B Chem. 267, 237–244. https://doi.org/10.1016/j.snb.2018.04.040.
Seshadri, P., Manoli, K., Schneiderhan-Marra, N., Anthes, U., Wierzchowiec, P., Bonrad, K., Di Franco, C., Torsi, L., 2018. Low-picomolar, label-free procalcitonin analytical detection with an electrolyte-gated organic field-effect transistor based electronic immunosensor. Biosens. Bioelectron. 104, 113–119. https://doi.org/10.1016/j.bios.2017.12.041.
Shalev, G., Landman, G., Amit, I., Rosenwaks, Y., Levy, I., 2013. Specific and label-free femtomolar biomarker detection with an electrostatically formed nanowire biosensor. NPG Asia Mater. 5, e41–7. https://doi.org/10.1038/am.2012.75.
Shalev, G., Rosenwaks, Y., Levy, I., 2012. The interplay between pH sensitivity and label-free protein detection in immunologically modified nano-scaled field-effect transistor. Biosens. Bioelectron. 31, 510–515. https://doi.org/10.1016/j.bios.2011.11.038.
Shen, N.Y.M., Liu, Z., Lee, C., Minch, B.A., Kan, E.C.C., 2003. Charge-based chemical sensors: a neuromorphic approach with chemoreceptive neuron MOS (CνMOS) transistors. IEEE Trans. Electron Devices 50, 2171–2178. https://doi.org/10.1109/TED.2003.816905.
Shoorideh, K., Chui, C.O., 2014. On the origin of enhanced sensitivity in nanoscale. PNAS 111, 5111–5116. https://doi.org/10.1073/pnas.1315485111.
Sipova, H., Zhang, S., Dudley, A.M., Galas, D., Wang, K., Homola, J., 2010. Surface plasmon resonance biosensor for rapid label-free detection of microribonucleic acid at subfemtomole level. Anal. Chem. 82, 10110–10115.
Song, J., Dailey, J., Li, H., Jang, H.-J., Russel, L., Zhang, P., Searson, P.C., Wang, J.T.H., Everett, A.D., Katz, H.E., 2018. Influence of bioreceptor layer structure on myelin basic protein detection using organic field effect transistor-based biosensors. Adv. Funct. Mater. 28, 1802605. https://doi.org/10.1002/adfm.201802605.
Song, J., Dailey, J., Li, H., Jang, H.J., Zhang, P., Wang, J.T.H., Everett, A.D., Katz, H.E., 2017. Extended solution gate OFET-based biosensor for label-free glial fibrillary acidic protein detection with polyethylene glycol-containing bioreceptor layer. Adv. Funct. Mater. 27. https://doi.org/10.1002/adfm.201606506.
Stern, E., Klemic, J.F., Routenberg, D.A., Wyrembak, P.N., Turner-Evans, D.B., Hamilton, A.D., LaVan, D.A., Fahmy, T.M., Reed, M.A., 2007a. Label-free immunodetection with CMOS-compatible semiconducting nanowires. Nature 445, 519–522. https://doi.org/10.1038/nature05498.
Stern, E., Wagner, R., Sigworth, F.J., Breaker, R., Fahmy, T.M., Reed, M.A., 2007b. Importance of the debye screening length on nanowire field effect transistor sensors. Nano Lett. 7, 3405–3409. https://doi.org/10.1021/nl071792z.
Stoop, R.L., Wipf, M., Müller, S., Bedner, K., Wright, I.A., Martin, C.J., Constable, E.C., Fu, W., Tarasov, A., Calame, M., Schönenberger, C., 2015. Competing surface reactions limiting the performance of ion-sensitive field-effect transistors. Sens. Actuators B Chem. 220, 500–507. https://doi.org/10.1016/j.snb.2015.05.096.
Torsi, L., Magliulo, M., Manoli, K., Palazzo, G., 2013. Organic field-effect transistor sensors: a tutorial review. Chem. Soc. Rev. 42, 8612–8628. https://doi.org/10.1039/c3cs60127g.
Tsai, M.H., Ma, T.P., 1994. The impact of device scaling on the current fluctuations in MOSFET's. IEEE Trans. Electron Devices 41, 2061–2068. https://doi.org/10.1109/16.333823.
van der spiegel, J., Lauks, I., Chan, P., Babic, D., 1983. The extended gate chemically sensitive field effect transistor as multi-species microprobe. Sens. Actuators 4, 291–298. https://doi.org/10.1016/0250-6874(83)85035-5.
Watanabe, S., Usui, K., Tomizaki, K., Mihara, H., 2005. Anomalous reflection of gold applicable for a practical protein-detecting chip platform. Mol. Biosyst. 1, 363–365. https://doi.org/10.1039/b513075c.
Wilk, G.D., Wallace, R.M., Anthony, J.M., 2001. High-κ gate dielectrics: current status and materials properties considerations. J. Appl. Phys. 89, 5243–5275. https://doi.org/10.1063/1.1361065.
Wisdom, G.B., 1976. Enzyme-immunoassay. Clin. Chem. 22, 1243–1255. https://doi.org/10.1016/0009-8981(77)90410-7.
Wu, M.H., Lin, T.W., Huang, M., De, Wang, H.Y., Pan, T.M., 2010. Label-free detection of serum uric acid using novel high-k Sm2TiO5 membrane-based electrolyte-insulator-semiconductor. Sens. Actuators B Chem. 146, 342–348. https://doi.org/10.1016/j.snb.2010.02.035.
Wu, T., Alharbi, A., You, K.-D., Kisslinger, K., Stach, E.A., Shahrjerdi, D., 2017. Experimental study of the detection limit in dual-gate biosensors using ultrathin silicon transistors. ACS Nano 7b02986. https://doi.org/10.1021/acsnano.7b02986.
Wunderlich, B.K., Neff, P.A., Bausch, A.R., 2007. Mechanism and sensitivity of the intrinsic charge detection of biomolecular interactions by field effect devices. Appl. Phys. Lett. 91, 18–20. https://doi.org/10.1063/1.2775040.
Wustoni, S., Hideshima, S., Kuroiwa, S., Nakanishi, T., Hashimoto, M., Mori, Y., Osaka, T., 2014. Sensitive electrical detection of human prion proteins using field effect transistor biosensor with dual-ligand binding amplification. Biosens. Bioelectron. 67, 256–262. https://doi.org/10.1016/j.bios.2014.08.028.
Yalow, R.S., Berson, S.A., 1960. Immunoassay of endogenous plasma insulin in man. J. Clin. Invest. 39, 1157–1175. https://doi.org/10.1172/JCI104130.
Yong, J., Jang, H., Cho, W., Islam, M.S., 2012. Highly sensitive electrolyte-insulator-semiconductor pH sensors enabled by silicon nanowires with Al2O3/SiO2 sensing membrane. Sens. Actuators B Chem. 171–172, 238–243. https://doi.org/10.1016/j.snb.2012.03.052.
Zafar, S., Emic, C.D., Afzali, A., Fletcher, B., Zhu, Y., Ning, T., 2011. Optimization of pH sensing using silicon nanowire field effect transistors with HfO2 as the sensing surface. Nanotechnology. https://doi.org/10.1088/0957-4484/22/40/405501.
Zhang, Q., Kaisti, M., Prabhu, A., Yu, Y., Song, Y.A., Rafailovich, M.H., Rahman, A., Levon, K., 2018. Polyaniline-functionalized ion-sensitive floating-gate FETs for the on-chip monitoring of peroxidase-catalyzed redox reactions. Electrochim. Acta 261, 256–264. https://doi.org/10.1016/j.electacta.2017.12.130.
Zhang, Q., Majumdar, H.S., Kaisti, M., Prabhu, A., Ivaska, A., Österbacka, R., Rahman, A., Levon, K., 2015. Surface functionalization of ion-sensitive floating-gate field-effect transistors with organic electronics. IEEE Trans. Electron Devices 62, 1291–1298.
Zhao, Y., Toyama, M., Kita, K., Kyuno, K., Toriumi, A., 2006. Moisture-absorption-induced permittivity deterioration and surface roughness enhancement of lanthanum oxide films on silicon. Appl. Phys. Lett. 88, 2004–2007. https://doi.org/10.1063/1.2174840.
Zhou, W., Dai, X., Fu, T., Xie, C., Liu, J., Lieber, C.M., 2014. Long term stability of nanowire nanoelectronics in physiological environments. Nano Lett. https://doi.org/10.1021/nl500070h.
Zhou, X., Wu, S., Liu, H., Wu, X., Zhang, Q., 2016. Nanomechanical label-free detection of aflatoxin B1 using a microcantilever. Sens. Actuators B Chem. 226, 24–29. https://doi.org/10.1016/j.snb.2015.11.092.